Am J Transl Res 2021;13(9):10014-10037
www.ajtr.org /ISSN:1943-8141/AJTR0131835

Original Article

ZLN005 protects against ischemia-reperfusion-induced kidney injury by mitigating oxidative stress through the restoration of mitochondrial fatty acid oxidation

Zhiyu Wang[1*], Zongjie Fu[2*], Chongjian Wang[1], Jing Xu[1], Hongkun Ma[1], Mengdi Jiang[1], Tingting Xu[1], Xiaobei Feng[1], Wen Zhang[1]

[1]Department of Nephrology, Ruijin Hospital, Shanghai Jiao Tong University School of Medicine, Shanghai 200025, China; [2]Department of Nephrology, Zhongshan Hospital, Fudan University, Shanghai 200032, China. [*]Equal contributors.

Received February 13, 2021; Accepted July 20, 2021; Epub September 15, 2021; Published September 30, 2021

Abstract: To date, the treatment of acute kidney injury (AKI) remains a difficult problem for clinicians. In the present study, we assessed whether ZLN005, a novel peroxisome proliferator-activated receptor-γ coactivator-1α (PGC-1α) agonist, can protect against ischemic AKI in vivo and in vitro. Notably, ZLN005 treatment significantly alleviated Ischemia-reperfusion (I/R)-induced tubular injury and reversed the decrease in hypoxia-reoxygenation-induced cell viability by restoring PGC-1α expression in a dose-dependent manner. This beneficial effect of ZLN005 was associated with the preservation of mitochondrial fatty acid oxidation (MitoFAO) and the alleviation of oxidative stress. Cotreatment with etomoxir, a specific inhibitor of carnitine palmitoyltransferase-1α (CPT-1α) activity, or CPT-1α siRNA abrogated ZLN005-induced antistress responses by mitigating reactive oxygen species production and decreasing apoptosis under ischemia-hypoxia conditions by suppressing MitoFAO. Further studies revealed that activation of endoplasmic reticulum (ER) stress may be involved in the effect of CPT-1α inhibition observed in vivo and in vitro. Collectively, our results suggest that ZLN005 confers a protective effect on I/R-induced kidney injury by mitigating ER stress through the restoration of MitoFAO by targeting PGC-1α.

Keywords: Acute kidney injury, peroxisome proliferator-activated receptor-γ coactivator-1α, ZLN005, carnitine palmitoyl transferase-1α, oxidative stress, apoptosis

Introduction

Acute kidney injury (AKI) is a global public health concern associated with high morbidity, mortality, and healthcare costs [1, 2]. Notably, other than dialysis, no therapeutic interventions reliably improve survival, limit injury, or speed recovery [1, 3]. Thus, new treatments for AKI are urgently needed.

Ischemia-reperfusion (I/R) injury due to low blood flow or sepsis is a common cause of AKI. Initial tissue damage caused by ischemia and hypoxia is aggravated during the reperfusion period through multiple mechanisms, including the activation of oxidative stress [4]. Subsequently, the activation of oxidative stress leads to the accumulation of reactive oxygen species (ROS) [5] and induces other adverse consequences, such as lipid peroxidation [6] and apoptosis [7]. Therefore, the identification of approaches to inhibit oxidative stress may aid in improving kidney outcomes after ischemic AKI.

Recent evidence has shown that mitochondrial fatty acid oxidation (MitoFAO) is involved in the regulation of oxidative stress and results in irreversible damage to tissues or cells [8-18]. However, the results of these studies are controversial. Some studies have demonstrated that excessive MitoFAO causes mitochondrial overload and subsequent ROS generation [8, 9], but others have shown that impaired MitoFAO also leads to the activation of oxidative stress [10-18]. In the I/R-induced AKI model, MitoFAO in renal tubular epithelial cells (RTECs) was shown to be substantially decreased [19-

21]. RTECs are high-energy-demanding cells that exhibit high levels of MitoFAO. In models of chronic kidney diseases, defective MitoFAO not only reduces ATP levels [22, 23], but also correlates with an imbalance in ROS production [24]. However, whether promoting MitoFAO inhibits oxidative stress and has positive effects in I/R-induced AKI remains unclear.

Peroxisome proliferator-activated receptor-γ coactivator-1α (PGC-1α) serves as a crucial coregulator that is expressed abundantly in RTECs to maintain energy homeostasis and mitochondrial biogenesis [25, 26]. Interestingly, a reduction in PGC-1α expression has been observed in I/R-, cisplatin- or lipopolysaccharide (LPS)-treated mouse kidneys [27-29]. In addition, PGC-1α knockout was shown to cause a notable reduction in FAO in the kidney by reducing the activity of the MitoFAO rate-limiting enzyme carnitine palmitoyltransferase-1α (CPT-1α) [28]. These results suggest that targeting PGC-1α may alleviate AKI by promoting the MitoFAO pathway. However, despite the potential benefits, no study has attempted to pharmacologically elevate PGC-1α levels and assess the subsequent effects in an I/R-induced AKI model. Recently, ZLN005, also known as 2-(4-tert-butylphenyl) benzimidazole, an activator of PGC-1α [30], was shown to exhibit protective effects under ischemic conditions by activating antioxidative enzymes in neurocytes [31]. Based on the curative effect of ZLN005 in treating ischemic disease and its potential to regulate MitoFAO and oxidative stress, the goal of the present study was to investigate whether ZLN005 can protect against I/R-induced kidney injury by inhibiting oxidative stress through an enhancement of MitoFAO.

Materials and methods

Animals and I/R-induced AKI models

Male C57BL/6 mice (10 weeks, 20-25 g) were purchased from Charles River Laboratories (Shanghai, China). All animals were housed in a standard environment and had free access to water and food. All procedures were conducted according to the NIH Guide for the Care and Use of Laboratory Animals published by the US National Academy of Sciences. The animal experiments were approved by the Animal Experiments Ethics Committee of Ruijin Hospital, Shanghai Jiao Tong University School of Medicine. Bilateral I/R surgery was performed on mice under anesthesia as previously described [32, 33]. Mice without renal pedicle clamping that underwent the same surgery were used as the sham group. After a 30-minute period of clamping of the bilateral renal pedicles, the clamps were released, and reperfusion lasted for 0, 2, 6, 12, 16, 24 or 48 h as indicated. Then, the mice were sacrificed when the reperfusion step was completed, and serum and renal cortex tissues were collected for further analysis.

Cell culture and hypoxia-reoxygenation (H/R) models

Human kidney tubular epithelial cells (HK2 cells, CRL-2190) were purchased from ATCC (Manassas, VA, USA) and routinely cultured in Dulbecco's modified Eagle's medium/nutrient mixture F-12 (DMEM/F12, Gibco, Waltham, MA, USA) containing 10% fetal bovine serum (FBS, Gibco). The cells were routinely cultured in an incubator under an atmosphere with 5% CO_2 at 37°C. For H/R modelling, after HK2 cell monolayers were grown to 50-60% confluence, they were subjected to starvation in serum-free medium for 24 h and then transferred to a hypoxic incubator (Thermo Electron, Waltham, MA, USA) under an atmosphere with 1% O_2, 5% CO_2 and 94% N_2 for another 24 h. After the hypoxic step, the cell dishes were transferred back to the normoxic incubator under an atmosphere with 21% O_2, and the culture medium was replaced with fresh medium supplemented with 10% FBS. The reoxygenation step lasted for 0, 2, 6, 12, 16, 24 or 48 h, and the cells were collected at the time points described above. Cells cultured in DMEM/F12 medium supplemented with 10% FBS without H/R were collected as the control samples.

Drug treatment

For *in vivo* experiments, the compounds ZLN005 (MedChemExpress, Monmouth Junction, NJ, USA) and etomoxir (Sigma-Aldrich, St. Louis, MO, USA) were dissolved in corn oil (MedChemExpress). ZLN005 was intraperitoneally injected into mice at doses of 3, 6 or 12 mg/kg, and etomoxir was intraperitoneally administered at a dose of 30 mg/kg. The mice were randomly divided into drug-treated and

nondrug-treated groups, with 4-8 mice in each group. The mice in the drug-treated group were intraperitoneally injected with one or two drugs 24 h before being sacrificed according to the experimental design. The mice in the nondrug-treated group were intraperitoneally injected with corn oil as a control. For *in vitro* experiments, ZLN005 and etomoxir were first dissolved in DMSO (Sigma-Aldrich) and then diluted with cell culture medium to obtain the proper concentration. Cells treated with an equal volume of DMSO were used as a control. After 24 h of hypoxia, the cells were treated with or without DMSO, ZLN005 (10, 20, or 40 μM) or 40 μM etomoxir for 24 h.

Transfection of CPT-1α siRNA

HK2 cells were cultured in six-well plates as monolayers. After reaching 50-60% confluence, the cells were transfected with 50 nM CPT-1α siRNA (Cat#: AM16708, IDs: 161677 and 161678, Thermo Fisher, Waltham, MA, USA) using Lipofectamine 3000 (Thermo Fisher). The volume of siRNA or Lipofectamine 3000 in each well was 5 μl, and after a 24-h transfection, the medium was discarded and replaced with fresh DMEM/F12 medium.

Renal function and histology

Renal function was measured by determining the level of serum creatinine (SCr) using a liquid chromatography tandem mass spectrometry (LC-MS/MS) method according to the instructions [34]. Kidney damage was evaluated by two experienced nephrologists in a blinded manner after hematoxylin-eosin (H&E) staining. The criteria for tubular damage included the loss of brush border, tubular dilation, cast formation and cell lysis [35]. The tubular damage score was calculated as the percentage of damaged tubules: >75% damage: 4 points; 50-75% damage: 3 points; 25-50% damage: 2 points; <25% damage: 1 point; no damage: 0 point.

Transmission electron microscopy (TEM)

The renal cortex tissues were cut into 1 mm^3 sections and quickly fixed in 2.5% glutaraldehyde. After being fixed in 1% osmium tetroxide and dehydrated in a graded ethanol series, the tissues were embedded in hard resin and cut into ultrathin slices (80 nm) using an ultramicrotome (Leica, Wetzlar, Germany). Before TEM observation, the slices were stained with uranyl acetate and lead citrate. For TEM, we primarily observed the number of lipid droplets and the structure of the mitochondria in proximal tubular epithelial cells. Mitochondrial damage includes mitochondrial fragmentation, swelling and crista fracture. To determine the degree of mitochondrial damage, at least 300 mitochondria from three different samples in each group were assessed.

Quantification of lipid peroxidation

Renal cortex tissue (10-20 mg) was homogenized in lysis buffer. Then, malondialdehyde (MDA) was extracted using a lipid peroxidation MDA Assay Kit (Beyotime, Shanghai, China) following the manufacturer's protocol. A microplate reader (Thermo Fisher) was used to detect the absorbance of each well at 535 nm. The calculated amounts of MDA were adjusted by tissue weight.

Western blot analysis

The renal cortex tissues and HK2 cells were lysed in RIPA lysis buffer (Millipore, Billerica, MA, USA) containing 10% PHOSSTOP (Roche, Basel, Switzerland) and 1% proteinase inhibitor (Thermo Fisher), and proteins were extracted following a previously described procedure [33]. For each sample, soluble proteins (20-30 μg) were loaded and separated by 10-12.5% sodium dodecyl sulfate-polyacrylamide gel electrophoresis before being transferred to a polyvinylidene difluoride (PVDF) membrane (Millipore). After being blocked with fast blocking buffer (EpiZyme, Shanghai, China) for 10-20 minutes, the PVDF membrane was incubated with specific primary antibodies overnight at 4°C. The primary antibodies were used at dilutions of 1:5000 for β-actin (Sigma-Aldrich), 1:1000 for PGC-1α (Proteintech, Wuhan, China), 1:1000 for CPT-1α (Proteintech), 1:2000 for B-cell lymphoma-2 (Bcl-2) (Abclonal, Wuhan, China), 1:2000 for Bcl-2-associated protein-X (Bax) (Abclonal), 1:1000 for cleaved caspase 3 (CC3, Cell Signaling Technology, Danvers, MA, USA), 1:2000 for phospho-Erk1/2 (Cell Signaling Technology) and 1:1000 for Erk1/2 (Cell Signaling Technology). Then, horseradish peroxidase (HRP)-conjugated secondary antibodies (Cell Signaling Technology) were incubated with the membrane at room temperature for 2 h.

The membranes were incubated with chemiluminescence HRP substrate (Millipore) and visualized with a chemiluminescence imaging system (Tanon, Shanghai, China). Stripping buffer (Beyotime) was used to remove antibodies from the PVDF membrane when detecting proteins of the same molecular weight. Grayscale analysis was used to quantify the proteins with ImageJ (National Institutes of Health), and β-actin was employed as an internal control for data analysis.

RNA extraction, reverse transcription, and quantitative reverse transcription PCR (qRT-PCR)

Total RNA was extracted from the renal cortex tissues and HK2 cells using TRIzol reagent (Thermo Fisher) following the manufacturer's instructions. The RNA concentration of each sample was determined with a NanoDrop 2000 system (Thermo Fisher), and 500 nmol of RNA was used for reverse transcription. Complementary DNA (cDNA) was then synthesized using an oligo PrimeScript™ RT Reagent Kit (TaKaRa, Shiga, Japan) following the manufacturer's instructions. Subsequently, the cDNA was diluted 10 times for qRT-PCR.

qRT-PCR was performed using the SYBR Premix Ex Tag Kit (TaKaRa) with the ABI 7500 Sequencing Detection System (Applied Biosystems, Foster City, CA, USA). Gene expression was calculated using the 2-ΔCt method, and β-actin was used as an internal control to normalize the relative values for each sample. The forward (F) and reverse (R) primers used to amplify target genes were as follows: mouse PGC-1α, F (5'-TATGGAGTGACATAGAGTGTGCT-3) and R (5'-CCACTTCAATCCACCCAGAAAG-3'); mouse CPT-1α, F (5'-CTCCGCCTGAGCCATGAAG-3') and R (5'-CACCAGTGATGATGCCATTCT-3'); mouse β-actin, F (5'-GTGACGTTGACATCCGTAAAGA-3') and R (5'-GCCGGACTCATCGTACTCC-3'); human PGC-1α, F (5'-TCTGAGTCTGTATGGAGTGACAT-3') and R (5'-CCAAGTCGTTCACATCTAGTTCA-3'); human CPT-1α, F (5'-TCCAGTTGGCTTATCGTGGTG-3') and R (5'-TCCAGAGTCCGATTGATTTTTGC-3'); and human β-actin, F (5'-CATGTACGTTGCTATCCAGGC-3') and R (5'-CTCCTTAATGTCACGCACGAT-3').

Immunohistochemistry (IHC) staining

Paraffin-embedded kidney sections (4-μm thick) were first subjected to heat-induced epitope retrieval at 75°C and then treated with peroxidase blocking solution and goat serum at room temperature. Subsequently, the sections were incubated with primary antibodies [anti-PGC-1α antibody (1:1000) or anti-CPT-1α antibody (1:1000)] overnight at 4°C and then with a biotinylated anti-IgG secondary antibody (Dako Omnis, Agilent Technologies, Santa Clara, CA, USA). Then, a DAB solution (Fuzhou Maixin, Fuzhou, Fujian, China) was used to detect the presence of HRP bound to the biotinylated secondary antibody, and the sections were imaged with an optical microscope (OM, Zeiss, Oberkochen, Germany).

Functional FAO assays

HK2 cells subjected to H/R and drug treatment were plated in poly-D-lysine-coated XF96 plates. Then, prior to analysis, the cells were starved for 12 h in medium supplemented with 1 mM glucose, 1 mM glutamine, 1% FBS and 0.5 mM L-carnitine to consume long-chain fatty acids. The rates of palmitate oxidation were measured by determining the oxygen consumption rate (OCR) using a Seahorse XFe96 analyzer following the manufacturer's instructions after the cells were incubated with Seahorse XF palmitate-BSA FAO reagents. The level of OCR was adjusted with respect to the number of cells seeded in each well.

Cell viability test

Cell Counting Kit-8 (CCK-8) assay was used to assess HK2 cell viability. Cells were seeded in 96-well cell culture plates and subjected to H/R injury with or without drug treatment according to the group. After 72 h of cultivation, the medium was discarded and replaced with 100 μl of fresh DMEM/F12 medium mixed with 10 μl of CCK-8 solution (Dojindo, Kumamoto, Kyushu, Japan). Then, the cells were incubated at 37°C for 2-4 h, and the absorbance was measured at 450 nm with a microplate reader. The cells in the group without any stimulation were set as the control (100%) to calculate the percent viability of HK2 cells. The effect of ZLN005 and etomoxir on cell viability was also evaluated with a Live/Dead Cell kit (Thermo Fisher). Cells were seeded in 24-well cell culture plates and cultured for 72 h with certain treatments. Then, the dye was prepared according to the instructions, and cells were treated with 100 μl of the

dye for 15 minutes in an incubator before being evaluated under a fluorescence microscope.

Detection of lipid droplets

Lipid probes were used to detect lipid droplets inside cells. Lipi-Red (100 nmol, Dojindo) was dissolved in 100 μl of DMSO to obtain a 1 mM stock solution, which was then diluted with serum-free medium to prepare a 5 μM working solution. HK2 cells were seeded in optical glass-bottomed dishes and cultured at 37°C for 30 minutes under different stimuli according to the group. Before analysis, the culture medium was removed, and the cells were washed twice with serum-free medium. Then, working solution was added and the cells were incubated at 37°C for 30 minutes in an incubator under an atmosphere with 5% CO_2. Subsequently, the samples were observed under a laser scanning confocal microscope (LSCM, LSM800, Zeiss) and imaged.

Mitochondrial membrane potential detection

MitoTracker Red CMXRos (Beyotime), a cell-permeable X-rosamine derivative (chloromethyl-X-rosamine, CMXRos), was used to assess mitochondrial membrane potential and specifically mark biologically active mitochondria in HK2 cells. MitoTracker Red CMXRos (50 μg) was dissolved in 470 μl of DMSO to obtain a 200 μM stock solution. The DMSO stock solution was next diluted with serum-free medium to prepare a 200 nM working solution, which was then added to the cell dishes and incubated at 37°C for 30 minutes in an incubator under an atmosphere with 5% CO_2. Subsequently, the samples were observed and imaged under a fluorescence microscope (OM, Zeiss).

Analysis of ROS

A hydrogen peroxide assay kit (Beyotime) was used to detect ROS levels in the kidney cortex according to the manufacturer's instructions. The absorbance was measured in a microplate reader at 560 nm, and the calculated amount of hydrogen peroxide (H_2O_2) was adjusted by tissue weight. For HK2 cells, ROS assay kit (Nanjing Jiancheng, Nanjing, Jiangsu, China) was used to measure ROS levels according to the manufacturer's instructions. Briefly, the cells were incubated with 10 μM dichlorodihydrofluorescein diacetate (DCFH-DA) for 15 minutes and then counterstained with Hoechst for 15 minutes to visualize the nuclei, with images obtained using a fluorescence microscope.

Detection of apoptosis

A TUNEL assay kit (Roche, Basel, Switzerland) was used to assess apoptosis in the paraffin-embedded renal sections, and 4',6-diamidino-2-phenylindole (DAPI) was used to counterstain the nuclei (blue fluorescence) prior to observing and imaging the samples by fluorescence microscopy.

Statistical analysis

All data are presented as the means ± SD. For the *in vivo* study, there were 4-6 mice in each group, and the assays were repeated three times. For the *in vitro* study, all assays were performed at least in triplicate, and the experiments were repeated three times. All data analyses were performed with GraphPad Prism (Version 5.0, GraphPad Software, San Diego, CA, USA). Comparisons between groups were performed with two independent samples t-tests, and differences were considered significant at $P<0.05$.

Results

I/R induces substantial tubular damage as well as changes in PGC-1α and CPT-1α expression

Renal I/R injury was assessed following the protocol described in **Figure 1A**. H&E staining revealed obvious tubular damage, including tubular vacuolization, loss of the brush border, tubular dilation, cellular necrosis, tubular cell detachment and cast formation (**Figure 1B**). The lesions were predominantly in the cortex and outer medulla junction. SCr levels gradually peaked at 3.49-fold of the baseline value in the first 24 h of reperfusion followed by a decrease after 48 h of reperfusion (**Figure 1C**), with the tubular damage score paralleling the observed change in SCr levels (**Figure 1D**). TEM images (**Figure 1E**) showed that the proximal RTECs experienced severe damage to the mitochondria with dilated and fragmented mitochondria easily observed after 24 h of reperfusion. However, the mitochondrial status improved after 48 h of reperfusion. In addition,

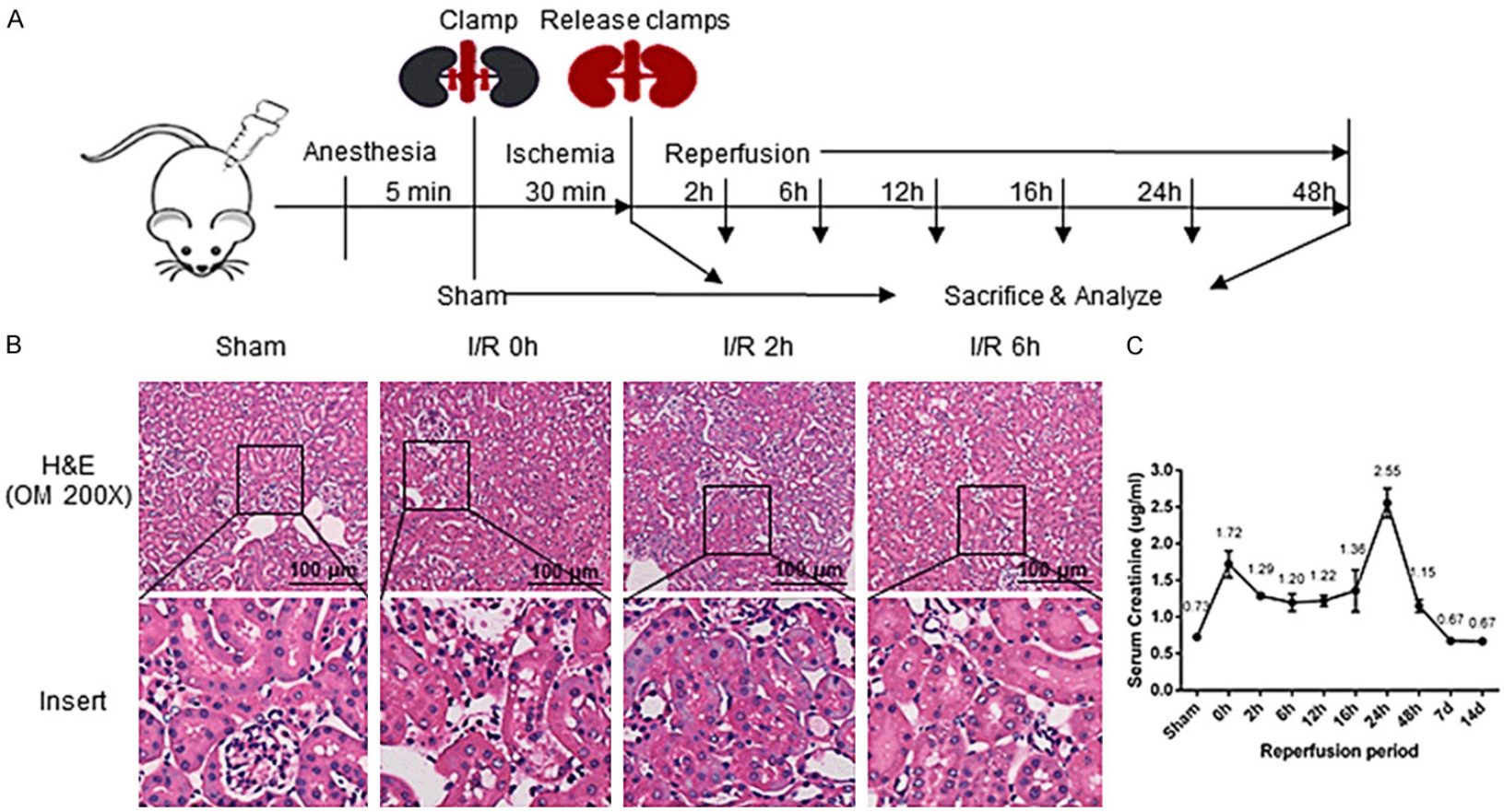
A
Clamp
Release clamps
Anesthesia
5 min
Ischemia
30 min
Reperfusion
2h
6h
12h
16h
24h
48h
Sham
Sacrifice & Analyze
B
Sham
I/R 0h
I/R 2h
I/R 6h
H&E
(OM 200X)
Insert
100 μm
C
Serum Creatinine (ug/ml)
3.0
2.5
2.0
1.5
1.0
0.5
0.0
0.73
1.72
1.29
1.20
1.22
1.36
2.55
1.15
0.67
0.67
Sham
0h
2h
6h
12h
16h
24h
48h
7d
14d
Reperfusion period

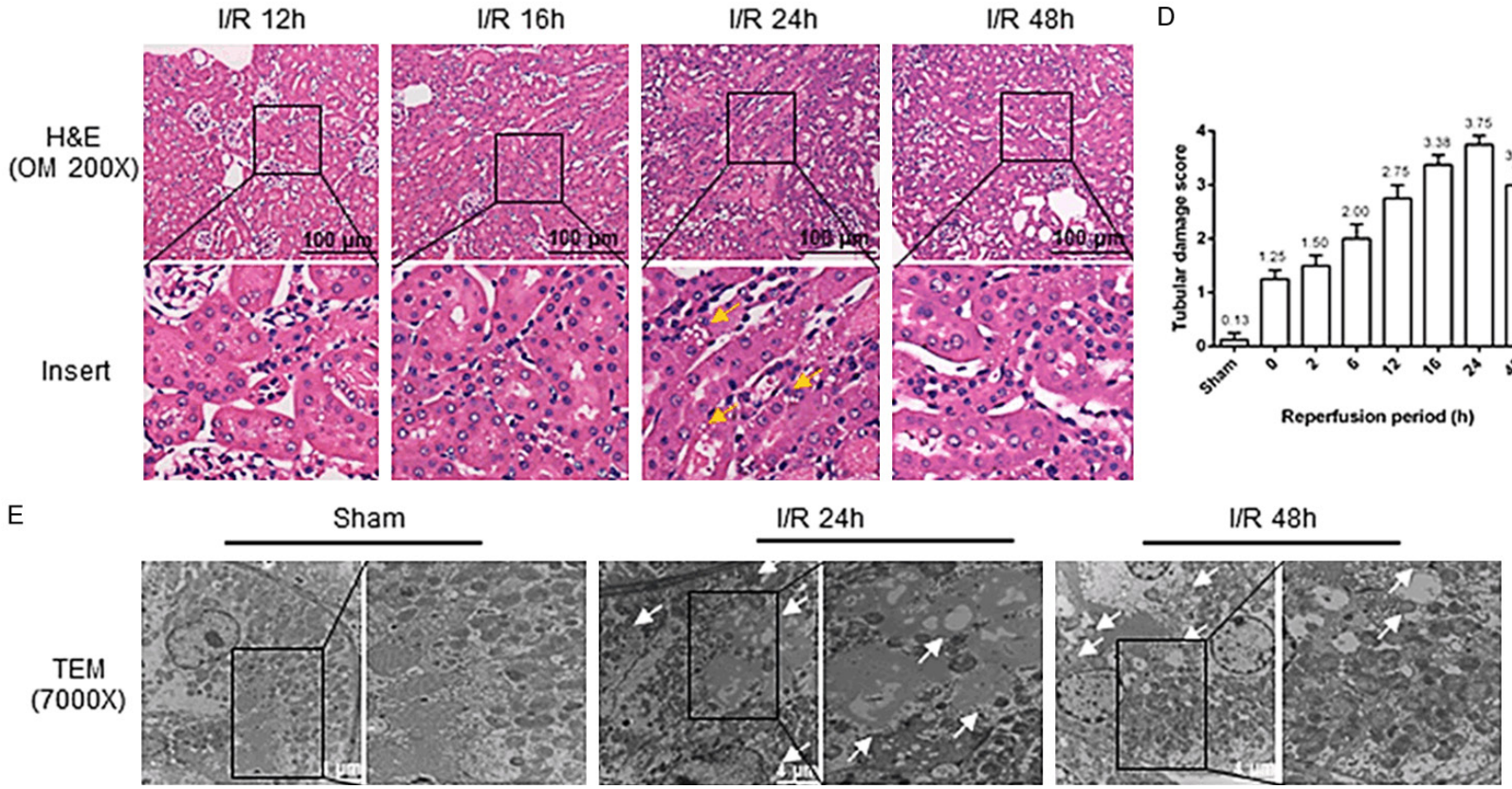

Figure 1. I/R induced kidney injury. A. Timeline scheme showing the procedures for I/R. Mice were subjected to 30 minutes of bilateral renal pedicles clamping followed by reperfusion for different periods of time (0, 2, 6, 12, 16, 24 or 48 h). Mice that received the same treatment without renal pedicle clamping were used as controls. B. Representative renal H&E staining images under an optical microscope (magnification of the upper panel, 200×; scale bar, 100 μm; the lower panel shows magnified images of the boxed areas in the upper panel). Yellow arrows, suspected lipid droplets. C. Summarized SCr levels. D. Summarized tubular damage scores. E. Representative TEM images (magnification of the left panel, 7000×; scale bar, 4 μm; the right panel shows magnified images of the boxed areas in the left panel left panel) of kidney tissues in the mice with or without I/R (24 or 48 h). White arrows, lipid droplets. n=6.

a strong accumulation of lipid droplets (white arrow) in proximal RTECs was observed after I/R, and a significant decrease in lipids was detected after 48 h of reperfusion compared to that observed after 24 h of reperfusion. These results indicated the successful generation of renal I/R injury in mice and revealed that tubular injury, including mitochondrial damage and lipid overload, reached the highest level after 24 h of reperfusion. We speculated that the severe metabolic disorder was closely related to the dysfunction of regulators of mitochondrial metabolism; therefore, we examined the level of PGC-1α, a critical coregulator of energy homeostasis and mitochondrial biogenesis, and its downstream factor CPT-1α, the MitoFAO rate-limiting enzymes located in the outer membrane of mitochondria [36], to investigate the cause of this phenomenon.

As shown in **Figure 2A**, **2B**, during renal I/R injury, the PGC-1α protein in renal cortex tissues was significantly decreased after ischemia and reached minimum levels after 24 h of reperfusion followed by an increase after 48 h of reperfusion. The IHC staining results showed that the PGC-1α protein was present in both the cytoplasm and nuclei of RTECs. After 24 h of reperfusion, the PGC-1α protein level in nuclei substantially decreased but was partly restored after 48 h of reperfusion (**Figure 2C**). The qRT-PCR results showed that the relative level of PGC-1α mRNA in the renal cortex changed in parallel with the PGC-1α protein during I/R injury (**Figure 2D**). Similarly, the CPT-1α protein and mRNA levels also gradually decreased and reached minimum levels after 24 h of reperfusion, and were partly restored after 48 h of reperfusion (**Figure 2E-H**). In summary, the changes in PGC-1α and CPT-1α expression paralleled the change in tubular injury during I/R, suggesting that increased PGC-1α expression may be involved in renal tubule self-repair in renal I/R-injured mice.

ZLN005 ameliorates I/R-induced kidney injury concomitant with reductions in oxidative stress and apoptosis after a single injection by elevating PCG-1α and CPT-1α levels in a dose-dependent manner

Based on the results described above, we injected the mice with the PGC-1α agonist ZLN005 (3-12 mg/kg) 24 h before they were sacrificed, after which the protein and mRNA levels of PGC-1α and its downstream factor CPT-1α were evaluated and shown to be elevated in a dose-dependent manner in renal cortex tissues (**Figure 3**).

Histological analysis of kidney cortex tissues showed that when administered to mice without I/R, ZLN005 treatment caused slight tubular injury. However, for the I/R-treated mice, a dose of 12 mg/kg ZLN005 effectively reduced tubular vacuolization, dilation and cell lysis after both 24 and 48 h of reperfusion (**Figure 4A**). In addition, the tubular damage and SCr scores showed the greatest decrease in the mice treated with 12 mg/kg ZLN005 (**Figure 4B**, **4C**). Considering that more benefits may be achieved with early treatment, we chose 24 h of reperfusion (also the time at which PGC-1α dropped to its lowest level in the I/R procedure) as the intervention time point and selected 12 mg/kg as the optimum concentration for ZLN005 treatment in the subsequent animal experiments.

To confirm whether ZLN005 can protect RTECs from ischemia- and hypoxia-induced oxidative stress, we examined the levels of H_2O_2 extracted from the renal cortex. As shown in **Figure 4D**, H_2O_2 levels in renal cortex tissues were significantly elevated after I/R injury, while ZLN005 treatment partly reversed this increase. Similar changes were observed for another marker of lipid peroxidation, MDA, in the I/R-injured and ZLN005-treated mice (**Figure 4E**). In addition, the TUNEL assay results showed that I/R-induced apoptosis was reduced in ZLN005-treated mice (**Figure 4F**), which may result from the mitigation of oxidative stress by ZLN005 treatment.

CPT-1α inhibition negates the beneficial effects of ZLN005 on oxidative stress and apoptosis

Etomoxir is a potent inhibitor of CPT-1α that irreversibly binds to its catalytic site and inhibits its activity [37, 38]. According to previous studies, 30 mg/kg etomoxir administered by intraperitoneal injection and 40 μM etomoxir in cell culture medium can inhibit MitoFAO [38, 39]. Therefore, we used 30 mg/kg etomoxir *in vivo* and 40 μM etomoxir *in vitro* alone or in combination with ZLN005 treatment to assess whether MitoFAO is required for the protective

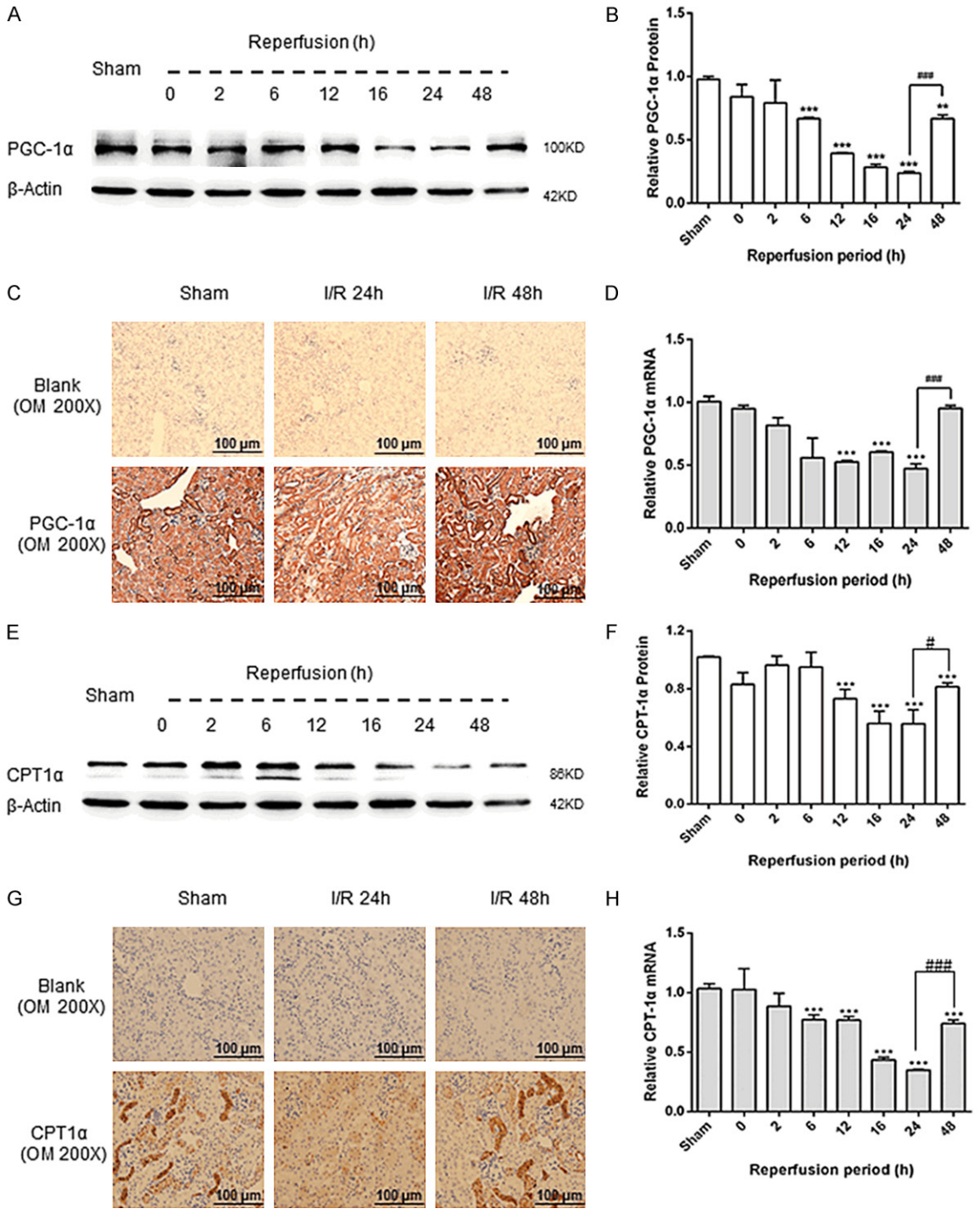

Figure 2. Changes in PGC-1α and CPT-1α in the renal cortex during I/R-induced kidney injury. (A) Representative Western blot images and (B) summarized data showing the time-dependent effect of reperfusion on PGC-1α protein levels. (C) Representative IHC staining image showing PGC-1α protein localization (magnification under an optical microscope, 200×; scale bar, 100 μm). (D) Summarized qRT-PCR data of PGC-1α mRNA expression in the renal cortex. (E) Representative Western blot images and (F) summarized data showing the time-dependent effect of reperfusion on CPT-1α protein expression. (G) Representative IHC staining image showing CPT-1α protein localization (magnification under an optical microscope, 200×; scale bar, 100 μm). (H) Summarized qRT-PCR data of CPT-1α mRNA expression in the renal cortex. n=6. $^{*}P<0.05$, $^{**}P<0.01$, $^{***}P<0.001$ vs. the control for PGC-1α and CPT-1α. $^{\#}P<0.05$, $^{\#\#\#}P<0.001$ vs. the I/R 24 h group.

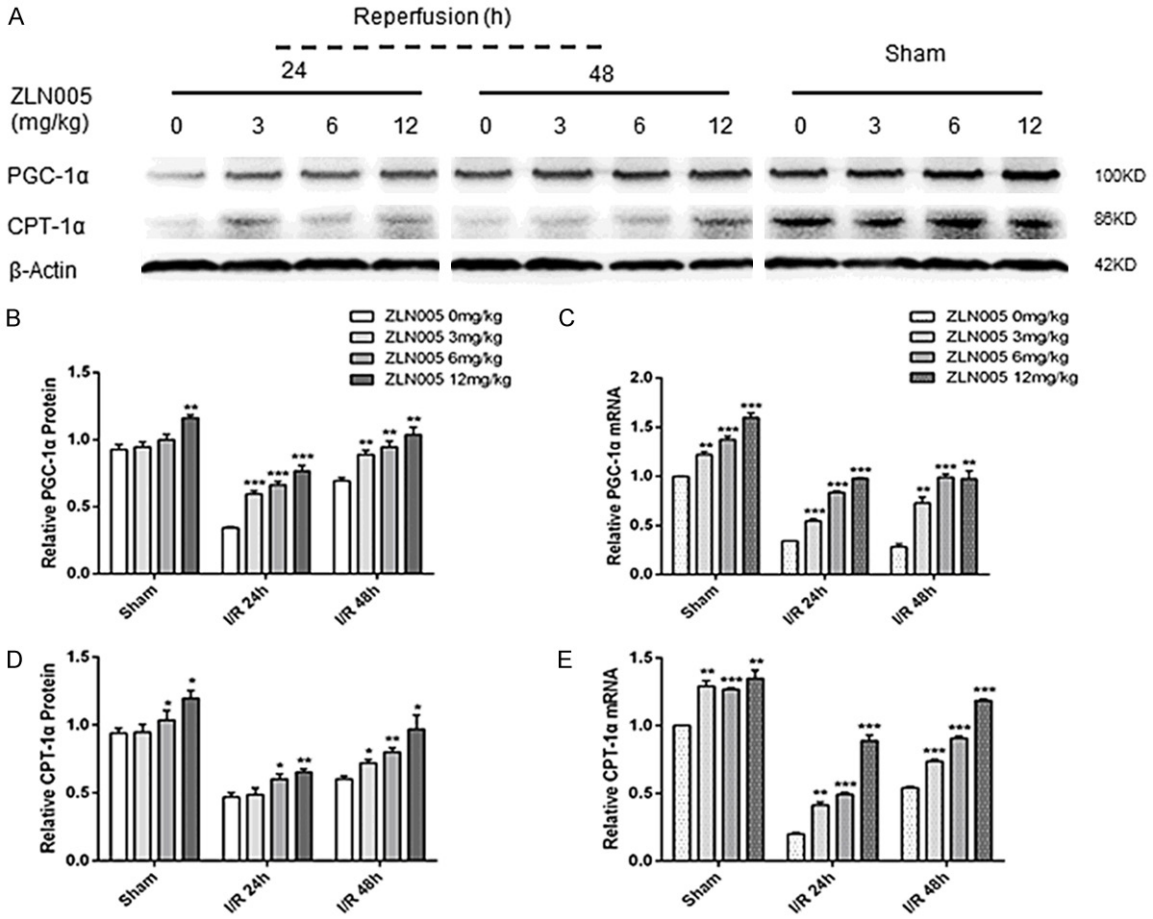

Figure 3. ZLN005 upregulated PGC-1α and CPT-1α expression in a dose-dependent manner. (A) Representative Western blot images and (B, D) summarized data showing the dose-dependent effect of ZLN005 (0, 3, 6, 12 mg/kg) treatment on PGC-1α and CPT-1α protein expression. (C) Summarized data of PGC-1α mRNA expression in the renal cortex of mice intraperitoneally administered 0, 3, 6 or 12 mg/kg ZLN005. (E) Summarized data of CPT-1α mRNA expression in the renal cortex of mice intraperitoneally administered 0, 3, 6 or 12 mg/kg ZLN005. n=4-6. *P<0.05, **P<0.01, ***P<0.001 vs. the control injected with corn oil.

effect of ZLN005. As shown in **Figure 5A**, the mice cotreated with etomoxir developed more severe tubular injury, increased lipid accumulation and greater mitochondrial damage than the mice administered a single treatment of ZLN005. Cotreatment with etomoxir notably abrogated the ability of ZLN005 to mitigate tubular damage and decrease the level of oxidative stress (**Figure 5B-D**).

Notably, ZLN005 treatment significantly reduced apoptosis in I/R-injured kidneys, as demonstrated by the TUNEL assay results (**Figure 5E**). Bcl-2 and Bax are crucial integrators of signals for cell survival and death. Bcl-2 has been confirmed to have antiapoptotic functions, while Bax has proapoptotic functions [40]. These two proteins are fully functional only when they are located on membranes of the endoplasmic reticulum (ER) or mitochondria [41]. In the present study, we measured the ratio of Bcl-2/Bax and the level of the apoptotic effector CC3 in renal cortex tissues. **Figure 5F** and **5G** shows that the Bcl-2/Bax ratio was significantly elevated and the level of CC3 was substantially decreased following ZLN005 treatment in the renal cortex tissues after I/R injury, a benefit that could be partly offset by the addition of etomoxir.

Since inhibiting fatty acid β-oxidation in mitochondria will reduce the generation of acetyl-CoA, which is used in the tricarboxylic acid cycle to produce ROS, the addition of etomoxir or CPT-1α siRNA should lead to decreased ROS production. However, the evidence described

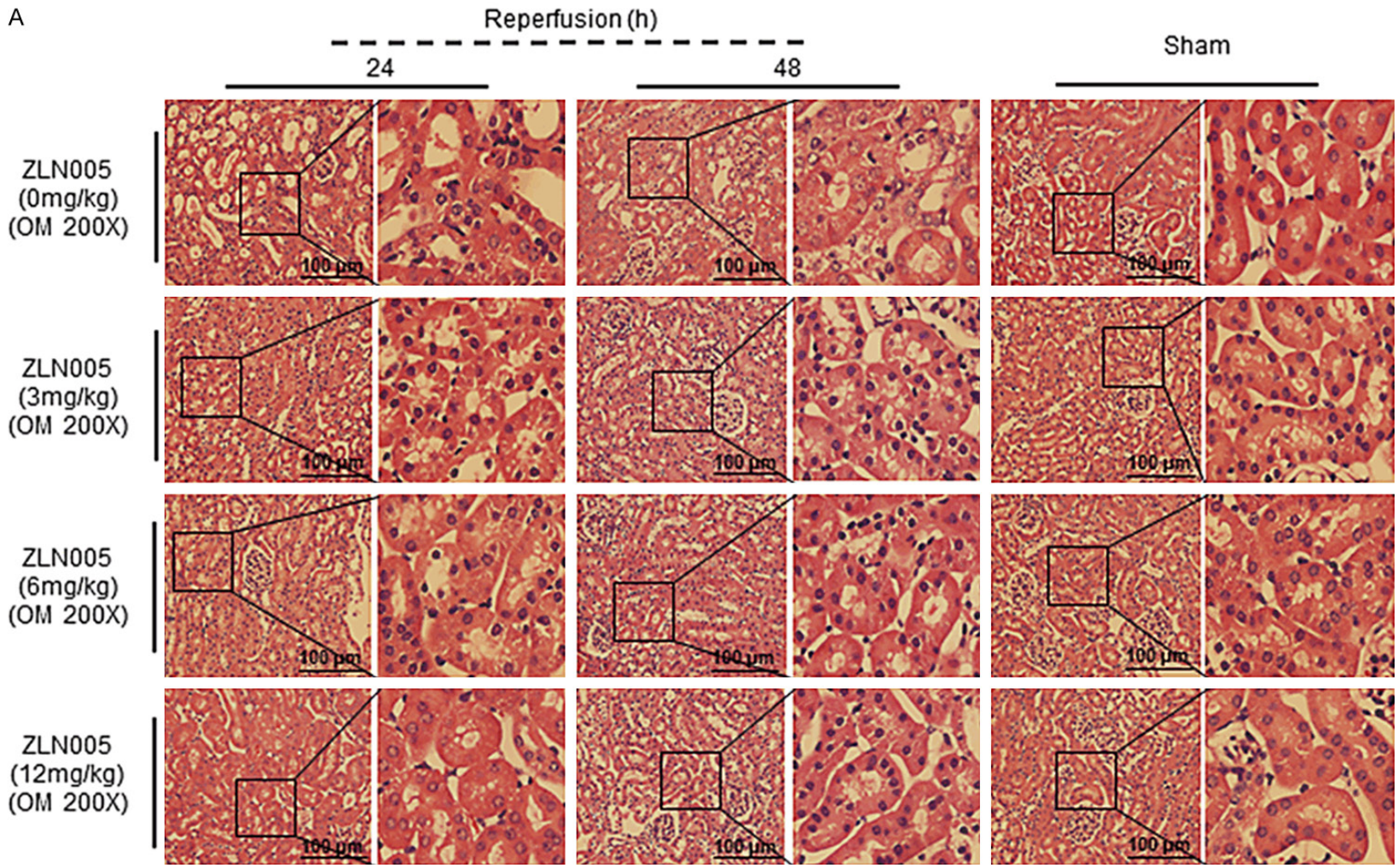
A
Reperfusion (h)
24
48
Sham
ZLN005
(0mg/kg)
(OM 200X)
ZLN005
(3mg/kg)
(OM 200X)
ZLN005
(6mg/kg)
(OM 200X)
ZLN005
(12mg/kg)
(OM 200X)
100 μm

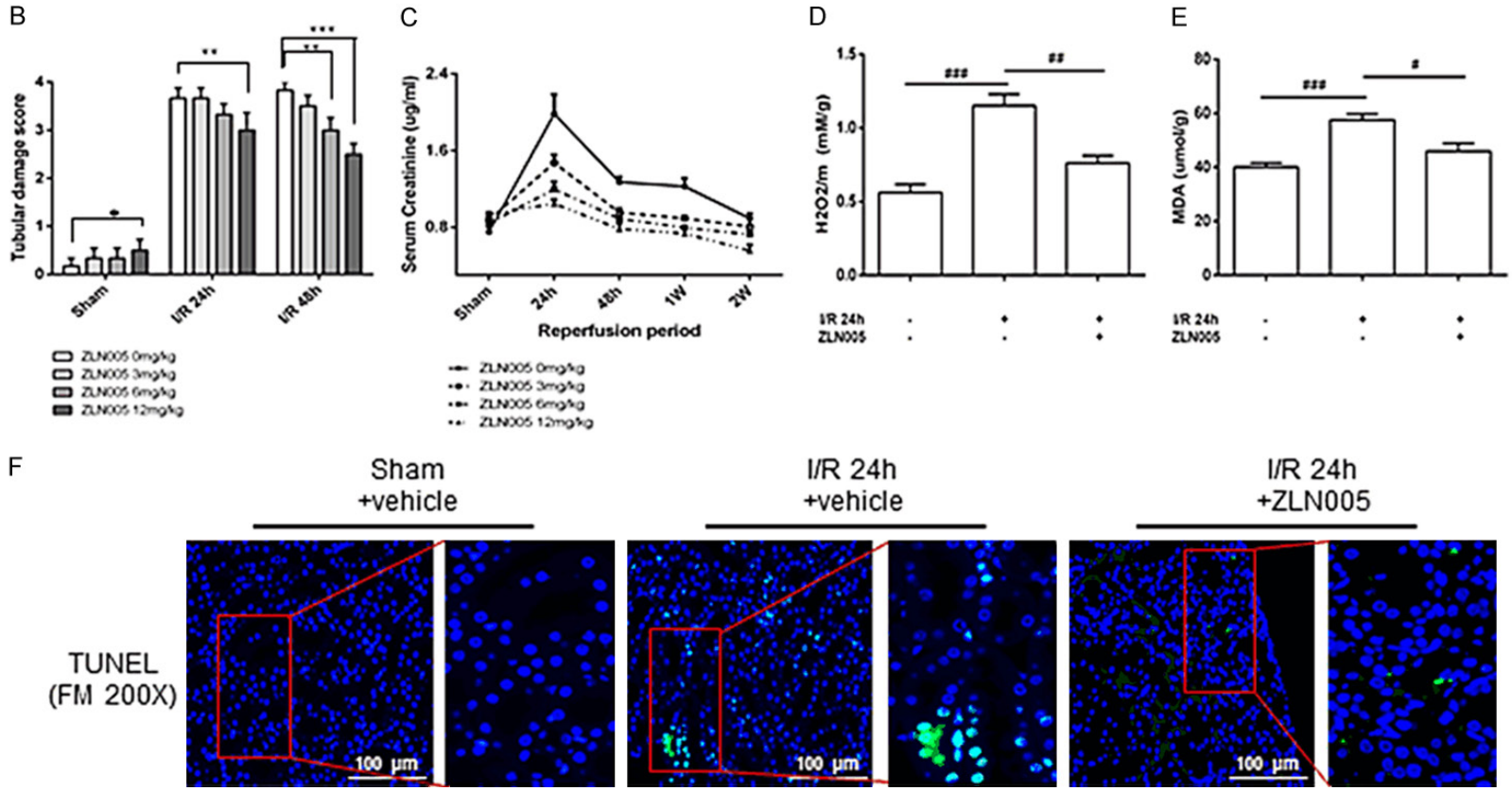

Figure 4. ZLN005 improves renal tubular injury and decreases oxidative stress and apoptosis in I/R-injured kidneys. (A) Representative renal H&E staining images under an optical microscope (magnification of the left panel, 200×; scale bar, 100 μm; the right panel shows magnified images of the boxed areas in the left panel) showing the dose-dependent effect of ZLN005 treatment (0, 3, 6, 12 mg/kg) on I/R induced renal tubular injury. (B) Summarized tubular damage scores. (C) Summarized SCr levels. (D) Summarized levels of H_2O_2 and (E) MDA extracted from the mouse renal cortex. (F) Representative images of cell apoptosis detected by TUNEL assay under a fluorescence microscope (magnification of the left panel, 200×; scale bar, 100 μm; the right panel shows magnified images of the boxed areas in the left panel). n=4-6. $^{\#}P<0.05$, $^{\#\#}P<0.01$, $^{\#\#\#}P<0.001$.

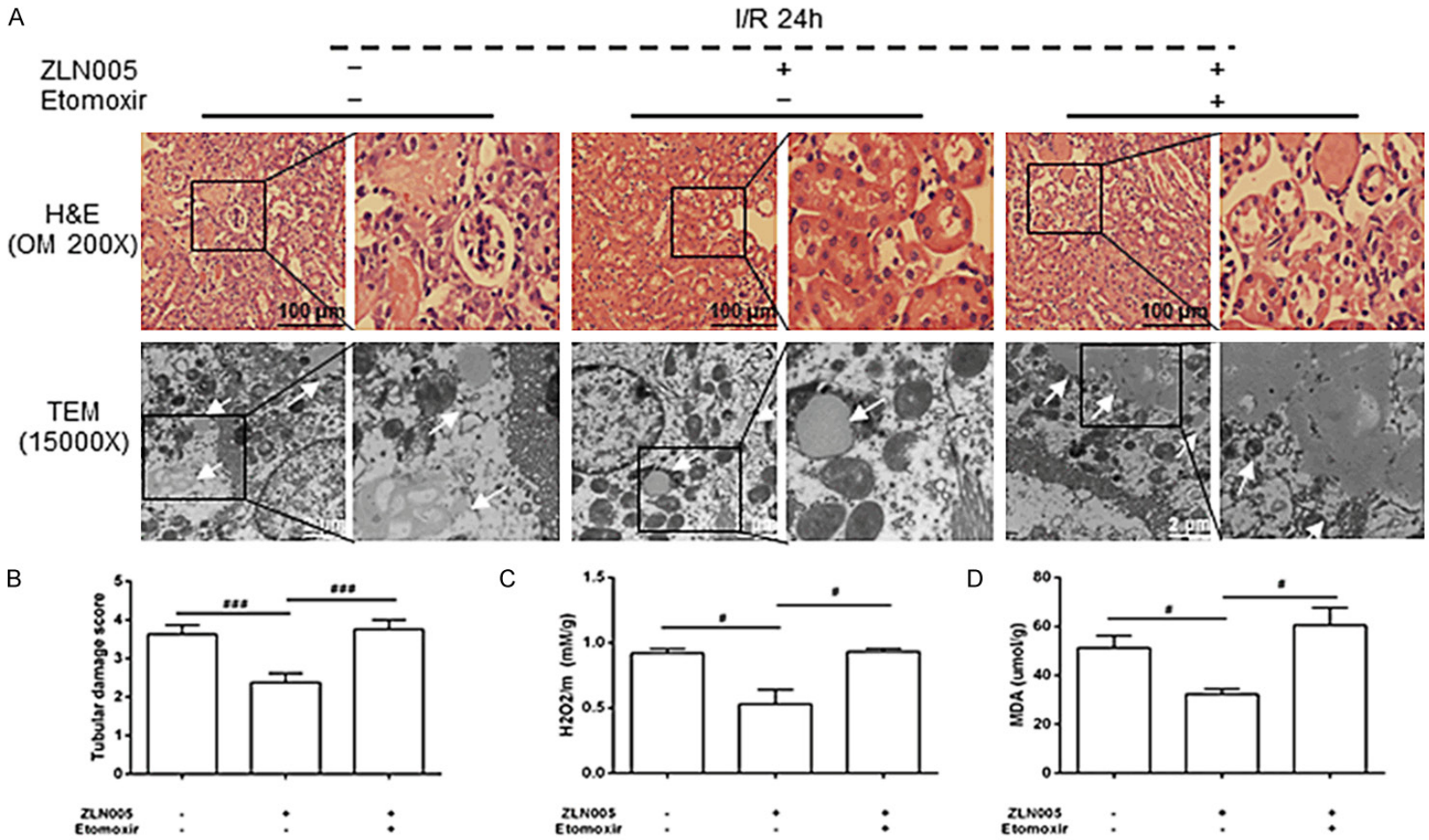
A
I/R 24h
ZLN005
Etomoxir
H&E
(OM 200X)
TEM
(15000X)
100 μm
2 μm
B
Tubular damage score
C
H2O2/m (mM/g)
D
MDA (umol/g)

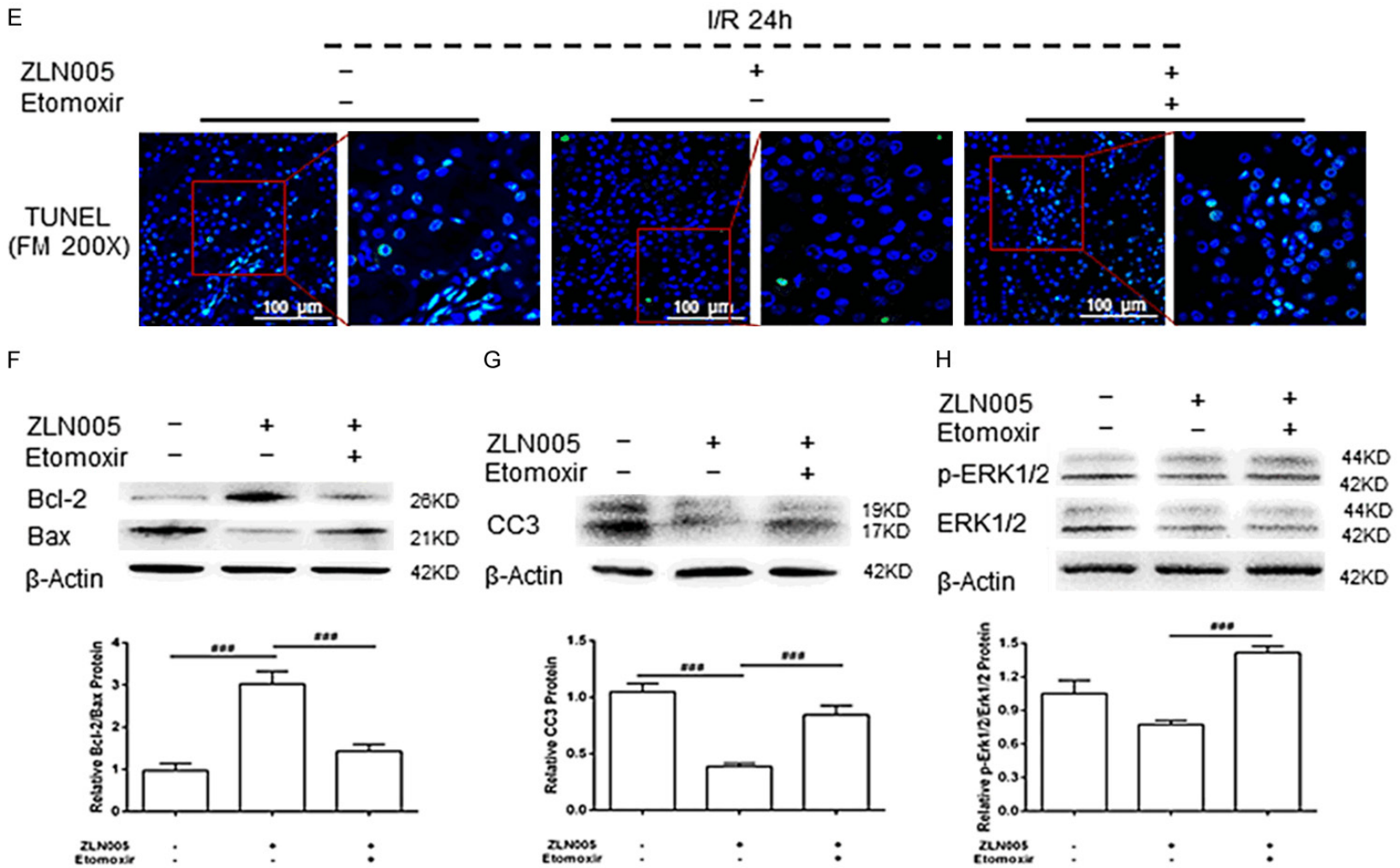

Figure 5. Inhibition of CPT-1α negates ZLN005-mediated changes in oxidative stress and apoptosis in I/R-injured kidneys. (A) Representative renal H&E staining images under an optical microscope (magnification of the left panel, 200×; scale bar, 100 μm; the right panel shows magnified images of the boxed areas in the left panel) and representative TEM images (magnification of the left panel, 15000×; scale bar, 2 μm; the right panel shows magnified images of the boxed areas in the left panel left panel) of kidney tissues in the I/R 24 h groups treated with ZLN005, ZLN005+etomoxir or neither. White arrows show lipid droplets. (B) Summarized tubular damage scores. (C) Summarized levels of H_2O_2 and (D) MDA extracted from the mouse renal cortex. (E) Representative images of cell apoptosis detected by TUNEL assays under a fluorescence microscope (magnification of the left panel, 200×; scale bar, 100 μm; the right panel shows magnified images of the boxed areas in the left panel). (F) Representative Western blot images and summarized data showing Bcl-2 and Bax expression and the ratio of Bcl-2 to Bax. (G) Representative Western blot images and summarized data showing CC3 expression. (H) Representative Western blot images and summarized data showing p-Erk1/2 levels. n=4-6. $^{\#}P<0.05$, $^{\#\#}P<0.01$, $^{\#\#\#}P<0.001$.

above revealed the opposite result. As ROS could originate from either the injured mitochondria or ER, we further measured the ratio of phosphorylated extracellular signal-regulated kinases 1/2 (p-ERK1/2) to extracellular signal-regulated kinases 1/2 (ERK1/2), a classic marker of ER stress, to determine whether the mitigation of ER stress is involved in the MitoFAO-mediated reduction in oxidative stress. **Figure 5H** shows that after the inhibition of CPT-1α, the level of ERK1/2 phosphorylation in I/R-injured RTECs was dramatically elevated, indicating that ER stress was reactivated in ZLN005-treated RTECs after cotreatment with etomoxir and that the antistress responses of the PGC-1α/CPT-1α axis in ischemic AKI may be associated with the suppression of ER stress. Collectively, these results showed that MitoFAO blockade counteracted the antistress responses in I/R-injured tubules induced by ZLN005 treatment, suggesting that MitoFAO is required for the improved antistress responses to I/R injury in RTECs mediated by ZLN005.

Effect of H/R on PGC-1α and CPT-1α expression in HK2 cells

We further evaluated whether H/R induces similar changes in PGC-1α and CPT-1α expression in HK2 cells by Western blot assay and qRT-PCR. **Figure 6A-F** shows that the mRNA levels of PGC-1α and CPT-1α were significantly decreased in HK2 cells after H/R stimulation. The protein levels of PGC-1α and CPT-1α paralleled the changes in mRNA levels. The transcription levels of the two genes were both reactivated after 48 h of reoxygenation, resulting in an increase in the protein level. Since the lowest levels of PGC-1α and CPT-1α in HK2 cells were observed after 24 h of reoxygenation, we evaluated the FAO and lipid levels at this time point. The FAO test results showed that the OCR was substantially decreased in HK2 cells exposed to 24 h of H/R stimulation after coculture with palmitate (**Figure 6G**) concomitant with a significant accumulation of lipid droplets as revealed by Lipi-Red staining (**Figure 6H**). These results suggested that H/R inhibited PGC-1α/CPT-1α signaling in renal tubular cells, thereby suppressing FAO and leading to lipid overload. Subsequently, PGC-1α/CPT-1α signaling was analyzed to confirm its role in H/R-induced HK2 cell injury.

ZLN005 treatment reverses H/R-induced ROS production and promotes cell viability by increasing PCG-1α and CPT-1α levels in a dose-dependent manner

We first performed a safety analysis using different doses of ZLN005 in routinely cultured HK2 cells. The results presented in **Figure 7A** show that ZLN005 treatment decreased cell viability at concentrations of 10 μM (although there was no significant difference) or higher in cell culture medium. HK2 cells were treated with 5 μM or lower levels of ZLN005 *in vitro*. Treatment with 2.5-5 μM ZLN005 significantly improved the viability of HK2 cells under H/R stimulation (**Figure 7B**, **7D**). In addition, ZLN005 treatment decreased the levels of ROS, lipid droplets and MDA that were increased by H/R (**Figure 7C**, **7D**). Besides, PGC-1α protein and mRNA levels in HK2 cells under H/R stimulation increased upon ZLN005 treatment in a dose-dependent manner (**Figure 7E-G**). Furthermore, CPT-1α protein and mRNA levels also notably increased when the cells were treated with 5 μM ZLN005 (**Figure 7H**, **7I**). Therefore, 5 μM ZLN005 was used in subsequent cell experiments.

CPT-1α inhibition abrogates the beneficial effects of ZLN005 treatment on oxidative stress and apoptosis

To further understand the role of CPT-1α in the beneficial effect of ZLN005 against H/R-induced ROS production, we used etomoxir, which inhibits CPT-1α activity, and siRNA targeting CPT-1α to inhibit the function of CPT-1α during the H/R procedure. Etomoxir (40 μM) effectively inhibited CPT-1α activity, as it significantly decreased the OCR of HK2 cells injected with palmitate (**Figure 8A**) while CPT-1α protein expression was notably knocked down by CPT-1α siRNA (**Figure 8B**, **8C**). Cotreatment with etomoxir or CPT-1α siRNA dramatically offset the ZLN005-mediated enhancement of cell viability (**Figure 8D**). The reduced benefits of ZLN005 caused by MitoFAO inhibition included increasing MDA levels (**Figure 8E**), promoting ROS production, decreasing mitochondrial membrane potential and aggravating lipid overload (**Figure 8F**). To determine whether blocking MitoFAO induces substantial adverse outcomes, we subsequently measured Bcl-2, Bax and CC3 levels to

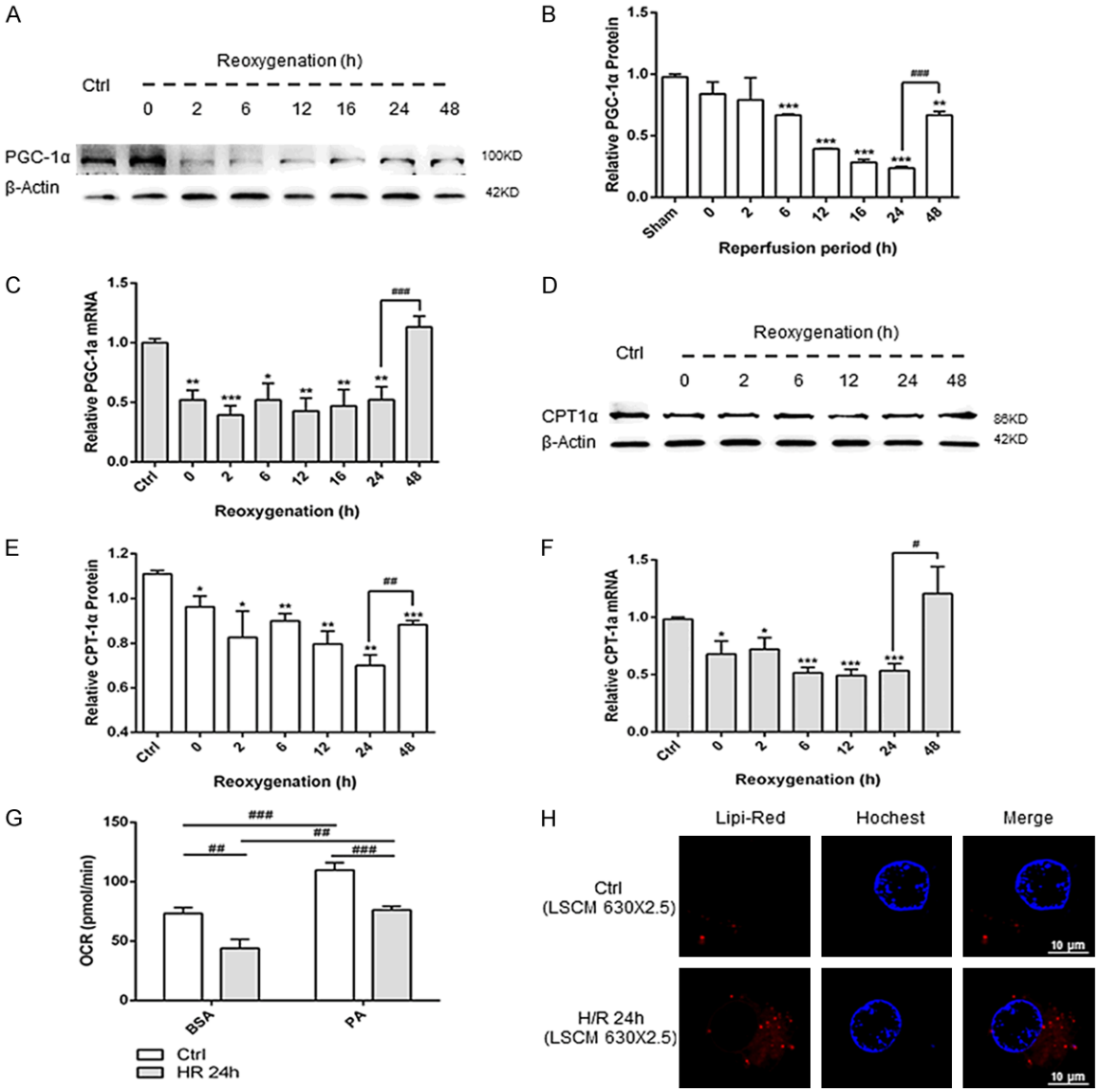

Figure 6. Changes in PGC-1α and CPT-1α expression in HK2 cells during H/R. (A) Representative Western blot images and (B) summarized data showing the time-dependent effect of H/R on PGC-1α protein expression. (C) Summarized qRT-PCR data of PGC-1α mRNA expression in H/R-stimulated HK2 cells. (D) Representative Western blot images and (E) summarized data showing the time-dependent effect of H/R on CPT-1α protein expression. (F) Summarized qRT-PCR data of CPT-1α mRNA expression in H/R-stimulated HK2 cells. (G) Summarized OCR data of HK2 cells in the control and H/R 24 h groups. (H) Representative images of lipid droplets detected with Lipi-Red in HK2 cells cultured under normoxia or H/R for 24 h (magnification under a confocal microscope, 630×2.5; scale bar, 10 μm). n=8-9. *P<0.05, **P<0.01, ***P<0.001 vs. the control for PGC-1α and CPT-1α. $^{\#}$P<0.05, $^{\#\#}$P<0.01, $^{\#\#\#}$P<0.001 vs. the H/R 24 h group.

assess whether CPT-1α inhibition counteracted the effect of ZLN005 on mitigating apoptosis induced by H/R. The results showed that cotreatment with etomoxir or CPT-1α siRNA effectively enhanced the level of apoptosis of ZLN005-treated HK2 cells without influencing PGC-1α levels (**Figure 9A-D**). In addition, the results presented in **Figure 9E** and **9F** show that after CPT-1α inhibition, ER stress was activated in the H/R-stimulated HK2 cells despite ZLN005 treatment. These results revealed that the alleviation of ER stress is an important part of the antistress responses of the PGC-1α/CPT-1α axis in an ischemic AKI model.

Discussion

In clinical practice, the treatment of AKI remains a difficult problem for clinicians despite the high level of attention given to this common dis-

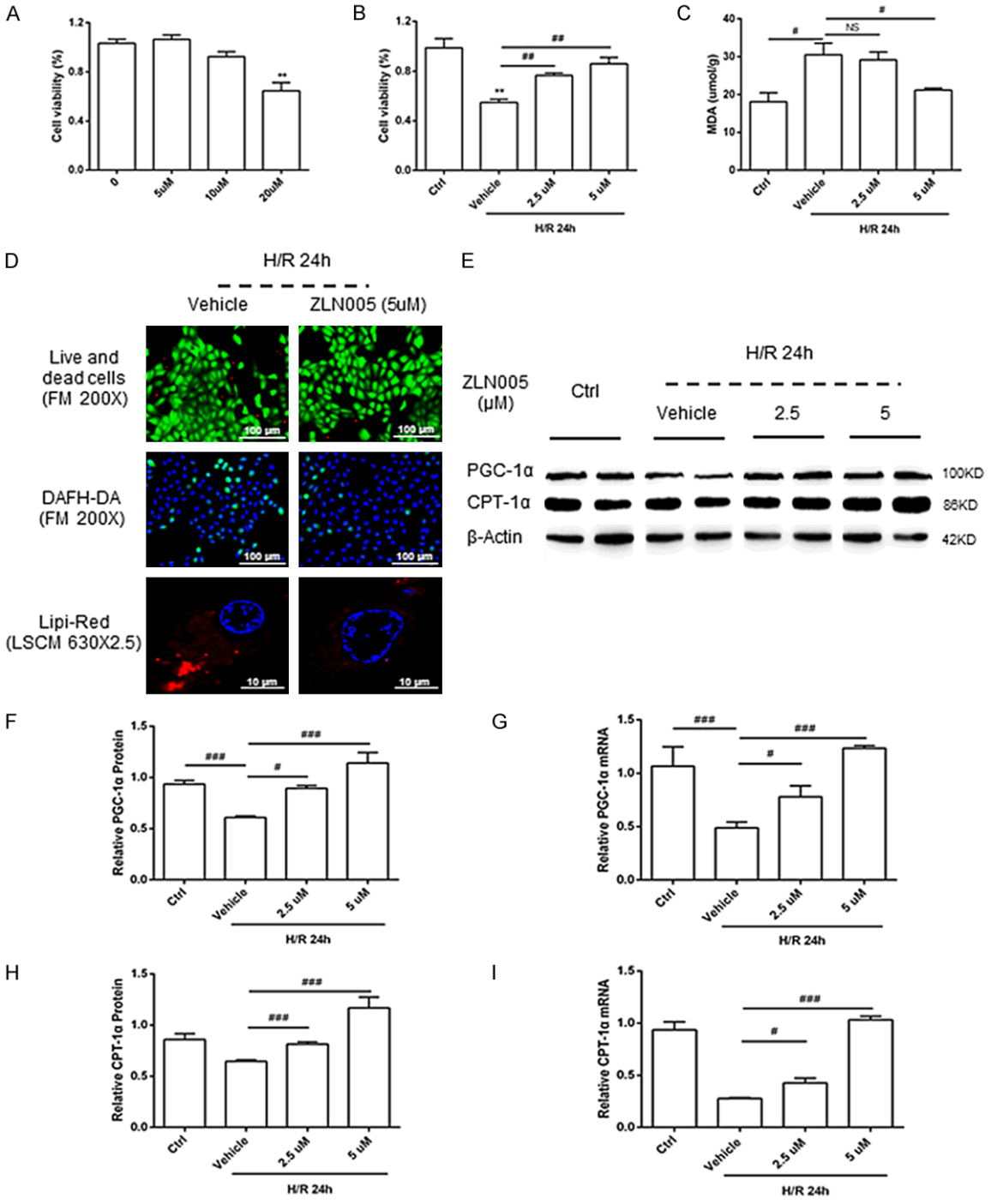

Figure 7. Effects of ZLN005 treatment on H/R-induced HK2 cell injury. (A) Summarized data of the viability of HK2 cells treated with 0, 5, 10 or 20 μM ZLN005 under normoxia to identify safe treatment concentrations. (B) Summarized data of the viability of HK2 cells cultured under normoxia or treated with 0, 2.5, or 5 μM ZLN005 under H/R conditions for 24 h. (C) Summary of MDA levels in HK2 cells cultured under normoxia or treated with 0, 2.5, or 5 μM ZLN005 under H/R for 24 h. (D) Representative images used to assess cell viability detected with a Live/Dead Cell Kit (magnification under fluorescence microscope, 200×; scale bar, 100 μm), ROS production detected by DAFH-DA (magnification under fluorescence microscope, 200×; scale bar, 100 μm) and lipid droplets detected by Lipi-Red (magnification under confocal microscope, 630×2.5; scale bar, 10 μm) of HK2 cells treated with or without 5 μM ZLN005 under H/R for 24 h. (E) Representative Western blot images and (F) summarized data showing the dose-dependent effect of ZLN005 on the H/R-induced decrease in PGC-1α protein expression. (G) Summarized data of relative PGC-1α mRNA levels in HK2 cells cultured under normoxia or treated with 0, 2.5, or 5 μM ZLN005

under H/R for 24 h. (H) Summarized data of CPT-1α protein levels in HK2 cells cultured under normoxia or treated with 0, 2.5, or 5 μM ZLN005 under H/R conditions for 24 h. (I) Summarized data of the relative CPT-1α mRNA levels in HK2 cells cultured under normoxia or treated with 0, 2.5, or 5 μM ZLN005 under H/R for 24 h. n=8-9, $^{NS}P\geq0.05$, $^{\#}P<0.05$, $^{\#\#}P<0.01$, $^{\#\#\#}P<0.001$.

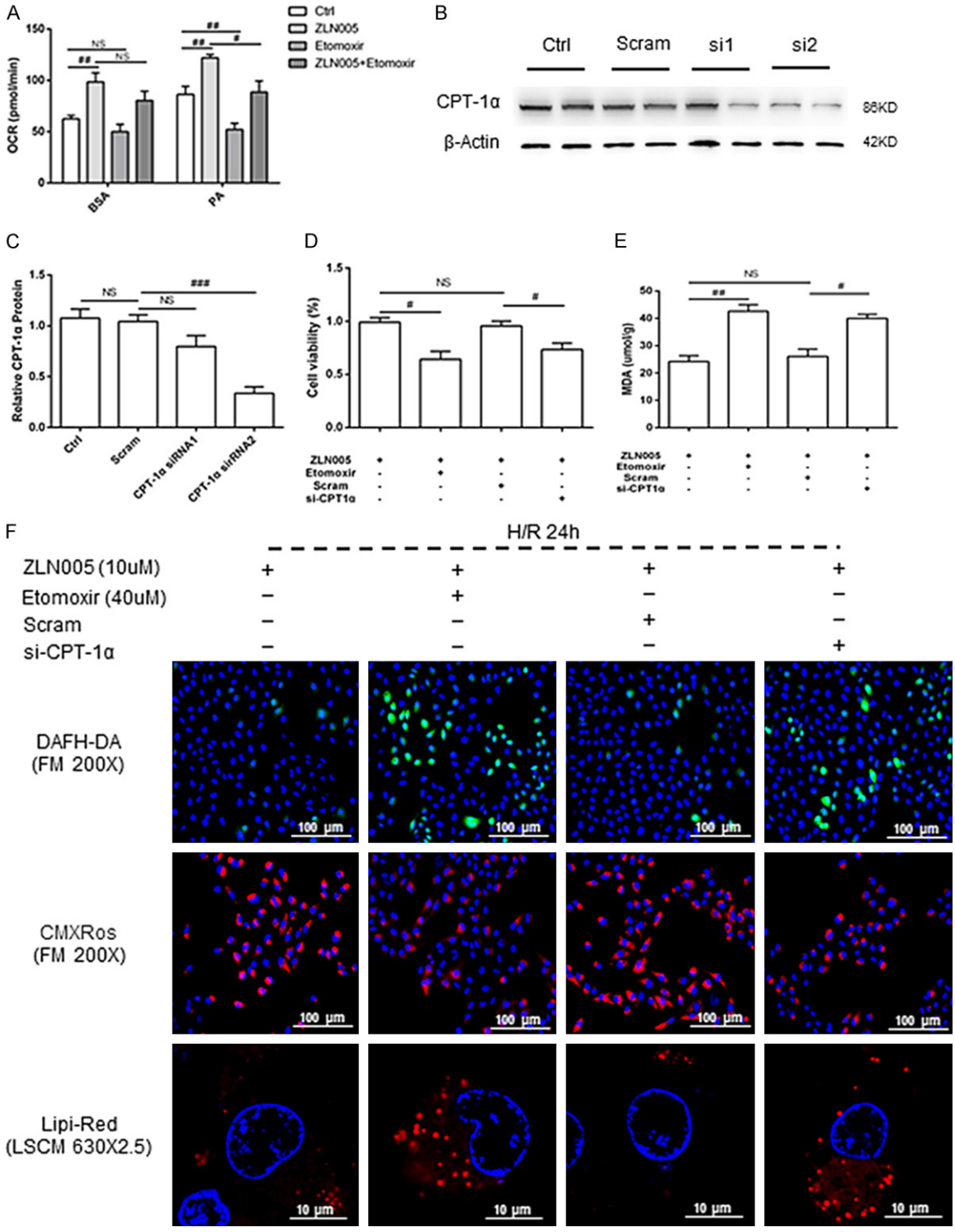

Figure 8. Inhibition of CPT-1α decreases the ZLN005-mediated benefits on oxidative stress in H/R-injured HK2 cells. (A) Levels of OCR in H/R-injured HK2 cells treated with ZLN005 with or without CPT-1α inhibition. (B) Representa-

tive Western blot images and (C) summarized data showing CPT-1α protein levels in HK2 cells treated with CPT-1α siRNA. (D) Summarized data of the viability of H/R-injured HK2 cells treated with ZLN005 with or without CPT-1α inhibition. (E) Summarized MDA levels in H/R-injured HK2 cells treated with ZLN005 with or without CPT-1α inhibition. (F) Representative images used to assess ROS production detected by DAFH-DA (magnification under a fluorescence microscope, 200×; scale bar, 100 μm), mitochondrial membrane potential detected by MitoTracker Red CMXRos (magnification under a fluorescence microscope, 200×; scale bar, 100 μm) and lipid droplets detected by Lipi Red (magnification under a confocal microscope, 630×2.5; scale bar, 10 μm) in H/R-injured HK2 cells treated with ZLN005 with or without CPT-1α inhibition. n=8-9, $^{NS}P\geq0.05$, $^{\#}P<0.05$, $^{\#\#}P<0.01$, $^{\#\#\#}P<0.001$.

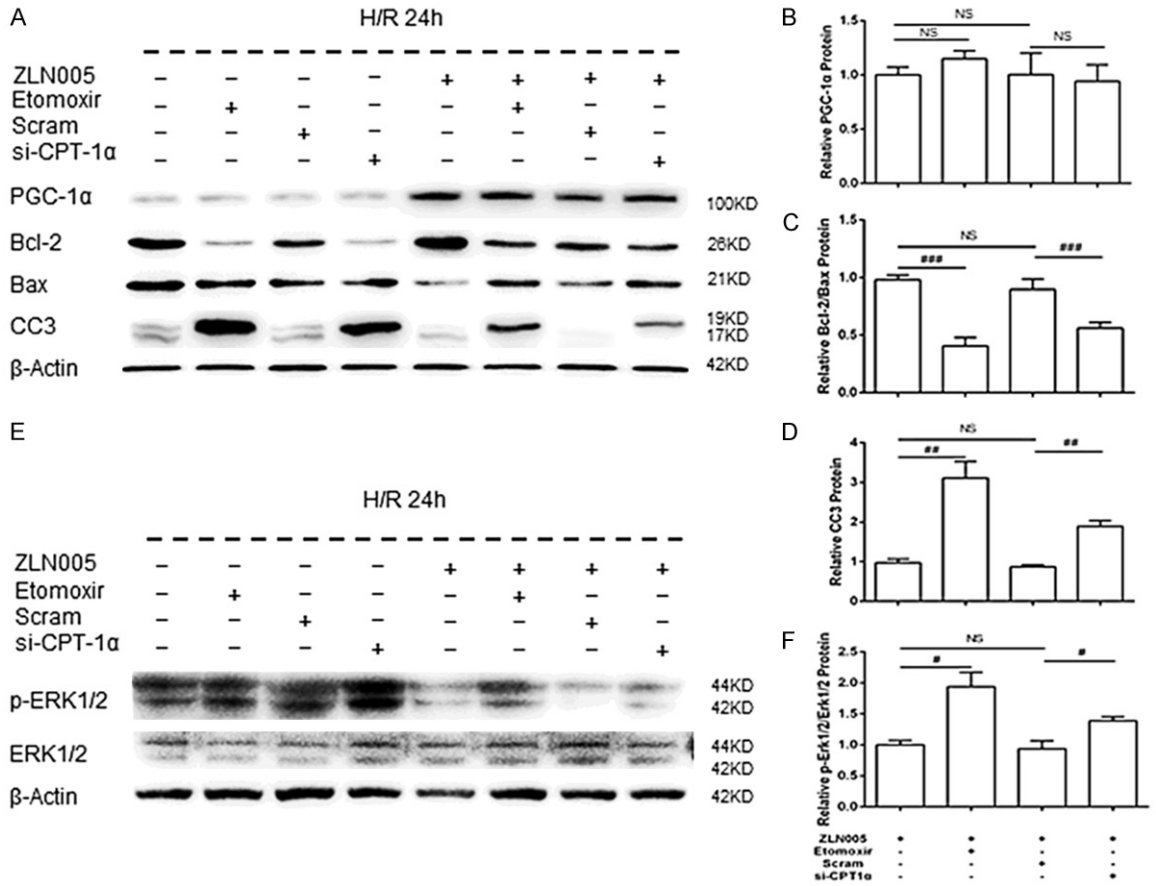

Figure 9. Inhibition of CPT-1α decreases the ZLN005-mediated benefits on apoptosis by activating ER stress in H/R-injured HK2 cells. (A) Representative Western blot images and (B-D) summarized data showing PGC-1α, Bcl-2, Bax and CC3 expression in HK2 cells with or without ZLN005 treatment and/or CPT-1α inhibition under H/R conditions for 24 h. (E) Representative Western blot images and (F) summarized data showing p-Erk1/2 levels in HK2 cells with or without ZLN005 treatment and/or CPT-1α inhibition under H/R conditions for 24 h. n=8-9, $^{NS}P\geq0.05$, $^{\#}P<0.05$, $^{\#\#}P<0.01$, $^{\#\#\#}P<0.001$.

ease [2]. Here, we provide new evidence that targeting PGC-1α may achieve some benefits in AKI treatment. In the present study, we successfully constructed ischemic AKI models *in vivo* and *in vitro* and performed a series of experiments to assess whether ZLN005, a PGC-1α agonist, can attenuate ischemic AKI. The results showed that ZLN005 treatment dose-dependently elevated PGC-1α and CPT-1α levels and reduced oxidative stress and apoptosis. Notably, the addition of etomoxir, an inhibitor of MitoFAO targeting CPT-1α, significantly abrogated the beneficial effect of ZLN005 on reducing oxidative stress and apoptosis in both I/R-induced AKI mice and H/R-induced HK2 cells. In addition, the transfection of CPT-1α siRNA effectively reversed the ZLN005-induced reduction in the levels of ROS, MDA and apoptosis in H/R-injured HK2 cells. Further studies revealed that the reactivation

of ER stress may be involved in the adverse effect of CPT-1α inhibition.

The pathophysiological procedure of I/R-induced kidney injury can be divided into two stages: the ischemia stage and the reperfusion stage. Ischemic renal injury is characterized by acute hypoxia due to the transient interruption of renal blood flow, whereas reperfusion is characterized by a sudden increase in oxygen concentration, resulting in increased ROS production and other oxidative stresses [42]. As a dominant and oxygen-dependent metabolic pathway, MitoFAO is immediately inhibited at the early stage of I/R [43]. As I/R injury progresses, the metabolic pattern of RTECs switches from aerobic to anaerobic and then back to aerobic. However, the suppression of MitoFAO may persist because of the inhibition of its associated enzymes, especially CPT-1α, even after a long period of reperfusion [44]. As a crucial coregulator of MitoFAO, PGC-1α is currently receiving increased attention. In our present study, we observed that PGC-1α levels changed with the duration of reperfusion. The PGC-1α mRNA and protein levels in the mouse renal cortex gradually decreased during the first 24 h of reperfusion after I/R but were spontaneously restored after 48 h of reperfusion. Interestingly, the change in PGC-1α expression paralleled the alteration of tubular injury and SCr during I/R, suggesting that increased PGC-1α levels may be involved in renal tubule self-repair in renal I/R-injured mice.

ZLN005 has been confirmed as a PGC-1α activator in skeletal muscle [30], vessels [45], brain [31], and cardiomyocytes [46, 47] and ZLN005 treatment has some benefits in ischemia-induced neuronal injury [31]. Given the curative potential of ZLN005, we performed a series of studies to test its effects on I/R-induced AKI. Our data demonstrated that ZLN005 has a dose-dependent pharmacological effect on PGC-1α transcription in I/R-injured mouse kidneys. Moreover, ZLN005 treatment showed benefits in restoring MitoFAO, lowering ROS and MDA levels, ameliorating mitochondrial damage and reducing apoptosis in I/R-injured RTECs, although high ZLN005 levels were toxic to HK2 cells with respect to cell viability. Thus, we believe that an appropriate dose of ZLN005 may be a potential treatment for ischemic AKI in the future.

In addition, the results of the present study provide evidence that MitoFAO activation might be a crucial factor in ZLN005-mediated antistress responses in ischemic AKI. The dysfunction of MitoFAO, an important mechanism of ATP production, can lead to adverse consequences under ischemic conditions, with imbalances in ROS production [48], mitochondrial damage [49] (including mitochondrial membrane potential reduction) and increased apoptosis [50] commonly observed. The finding that the beneficial effects resulting from ZLN005 treatment were dramatically counteracted by inhibiting the activity or expression of CPT-1α further confirmed the importance of restoring MitoFAO in RTECs after ischemic injury. The results also confirmed that CPT-1α is a downstream target of PGC-1α, supporting the results of several other recently published studies [51, 52]. In addition, our results showing that CPT-1α inhibition activates ERK1/2 phosphorylation revealed that the benefits of the ZLN005-mediated activation of the PGC-1α/CPT-1α axis in the ischemic AKI model were related to ER stress suppression. As the inhibition of CPT-1α limited the use of long-chain fatty acids, especially palmitate, excess palmitate would lead to uncontrolled lipotoxicity due to the exceeding amount that could be preserved in the lipid pool and result in subsequent alterations in phospholipid composition or other changes in membrane rigidity and fluidity [53, 54]. Thus, we conjectured that the inhibition of ER stress by ZLN005 may be attributed to a reduction in lipid accumulation and lipotoxicity. Similar findings were recently reported in studies of pancreatic acinar cells and hepatic cells [10, 15]. In summary, our findings demonstrated that ZLN005 protects against ischemic AKI by mitigating ER stress through the activation of PGC-1α/CPT-1α signaling.

There are a few limitations in the current study. First, the proper dose of etomoxir used in different studies is controversial [16, 38]. In the present study, we selected 30 mg/kg etomoxir for intraperitoneal injection and 40 μM etomoxir in cell culture medium to inhibit MitoFAO in an AKI model in accordance with the concentration used by other researchers when treating mice with kidney injury or proximal renal tubular cells [39]. Etomoxir may inhibit other proteins, such as mitochondrial adenine nucleotide transporters and complex I of the electron transport chain, thereby influencing

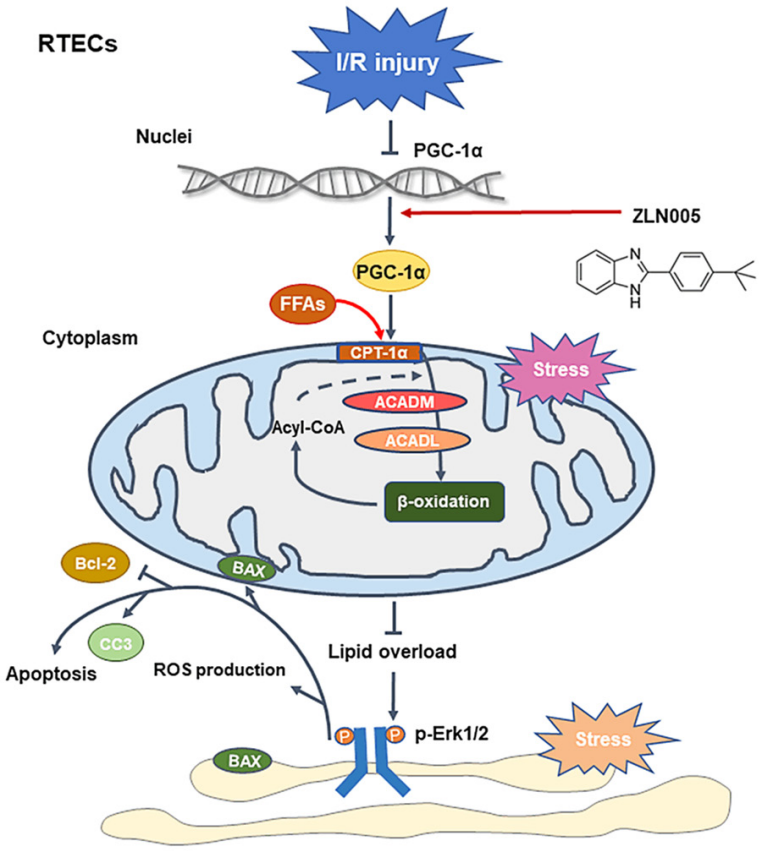

Figure 10. Diagram showing PGC-1α agonist ZLN005 restores MitoFAO to attenuate I/R-induced kidney injury by inhibiting oxidative stress and apoptosis.

the tricarboxylic acid cycle. In addition, we only evaluated the role of ZLN005 in ischemic AKI models. For translation of our findings to clinical applications in AKI, it's necessary to confirm the effect of ZLN005 in additional models of cisplatin- or LPS-induced AKI in future studies.

Conclusions

The results of our present study provide strong evidence that PGC-1α and CPT-1α expression is notably inhibited in an ischemic AKI model both *in vivo* and *in vitro*. Treatment with ZLN005 significantly elevated PGC-1α and CPT-1α levels and reduced oxidative stress. The blockade of MitoFAO by etomoxir was shown to offset the antistress responses induced by ZLN005 treatment in hypoxic-ischemic injured renal tubule epithelial cells by reactivating ER stress. In summary, although in-depth studies and pilot trials are still warranted, our findings suggest that ZLN005 treatment attenuates I/R-induced kidney injury by promoting antistress responses through an enhancement of MitoFAO by targeting PGC-1α (**Figure 10**).

Acknowledgements

This study was funded by the National Natural Science Foundation of China (grant number 81470967 and 81-670613).

Disclosure of conflict of interest

None.

Abbreviations

AKI, acute kidney injury; RTECs, renal tubular epithelial cells; PGC-1α, peroxisome proliferator-activated receptor-γ coactivator-1α; CPT-1α, carnitine palmitoyltransferase-1α; I/R, ischemia-reperfusion; ROS, reactive oxygen species; MitoFAO, mitochondrial fatty acid oxidation; H/R, hypoxia-reoxygenation; SCr, serum creatinine; LC-MS/MS, liquid chromatography tandem mass spectrometry; TEM, transmission electron microscopy; MDA, malondialdehyde; PVDF, polyvinylidene difluoride; qRT-PCR, quantitative reverse transcription PCR; IHC, immunohistochemistry; OCR, oxygen consumption rate; CCK-8, cell counting kit-8; CMXRos, chloromethyl-X-rosamine; H_2O_2, hydrogen peroxide; DCFH-DA, dichloro-dihydrofluorescein diacetate; HRP, horseradish peroxidase; Bcl-2, B-cell lymphoma-2; Bax, Bcl-2-associated protein-X; CC3, cleaved caspase 3; ER, endoplasmic reticulum; p-ERK1/2, phosphorylated extracellular signal-regulated kinases 1/2; ERK1/2, extracellular signal-regulated kinases 1/2; BSA, bovine serum albumin; PA, palmitate.

Address correspondence to: Drs. Wen Zhang and Xiaobei Feng, Department of Nephrology, Ruijin Hospital, Shanghai Jiao Tong University School of Medicine, Shanghai 200025, China. Tel: +86-021-

64370045-665233; E-mail: zhangwen255@163.com (WZ); fxb11116@rjh.com.cn (XBF)

References

[1] Zuk A and Bonventre JV. Acute kidney injury. Annu Rev Med 2016; 67: 293-307.

[2] Bellomo R, Kellum JA and Ronco C. Acute kidney injury. Lancet 2012; 380: 756-766.

[3] Mayeux PR and MacMillan-Crow LA. Pharmacological targets in the renal peritubular microenvironment: implications for therapy for sepsis-induced acute kidney injury. Pharmacol Ther 2012; 134: 139-155.

[4] Liao W, Fu Z, Zou Y, Wen D, Ma H, Zhou F, Chen Y, Zhang M and Zhang W. MicroRNA-140-5p attenuated oxidative stress in cisplatin induced acute kidney injury by activating Nrf2/ARE pathway through a Keap1-independent mechanism. Exp Cell Res 2017; 360: 292-302.

[5] Gorin Y. The kidney: an organ in the front line of oxidative stress-associated pathologies. Antioxid Redox Signal 2016; 25: 639-641.

[6] Lorenzen JM, Batkai S and Thum T. Regulation of cardiac and renal ischemia-reperfusion injury by microRNAs. Free Radic Biol Med 2013; 64: 78-84.

[7] Aksu U, Demirci C and Ince C. The pathogenesis of acute kidney injury and the toxic triangle of oxygen, reactive oxygen species and nitric oxide. Contrib Nephrol 2011; 174: 119-128.

[8] Shi J, Fu H, Jia Z, He K, Fu L and Wang W. High expression of CPT1A predicts adverse outcomes: a potential therapeutic target for acute myeloid leukemia. EBioMedicine 2016; 14: 55-64.

[9] Koves TR, Ussher JR, Noland RC, Slentz D, Mosedale M, Ilkayeva O, Bain J, Stevens R, Dyck JR, Newgard CB, Lopaschuk GD and Muoio DM. Mitochondrial overload and incomplete fatty acid oxidation contribute to skeletal muscle insulin resistance. Cell Metab 2008; 7: 45-56.

[10] Srinivasan MP, Bhopale KK, Caracheo AA, Amer SM, Khan S, Kaphalia L, Loganathan G, Balamurugan AN and Kaphalia BS. Activation of AMP-activated protein kinase attenuates ethanol-induced ER/oxidative stress and lipid phenotype in human pancreatic acinar cells. Biochem Pharmacol 2020; 180: 114174.

[11] Jersin R, Priyanka Tallapragada DS, Madsen A, Skartveit L, Fjære E, McCann A, Dyer L, Willems A, Bjune JI, Bjune MS, Våge V, Nielsen HJ, Thorsen HL, Nedrebø BG, Busch C, Steen VM, Blüher M, Jacobson P, Svensson PA, Fernø J, Rydén M, Arner P, Nygård O, Claussnitzer M, Ellingsen S, Madsen L, Sagen JV, Mellgren G and Dankel SN. Role of the neutral amino acid transporter Slc7a10 in adipocyte lipid storage, obesity and insulin resistance. Diabetes 2021; 70: 680-695.

[12] Wang W and Hu X. Mild hypothermia attenuates hepatic ischemia-reperfusion injury through regulating the JAK2/STAT3-CPT1a-dependent fatty acid β-oxidation. Oxid Med Cell Longev 2020; 2020: 5849794.

[13] Cabrero A, Merlos M, Laguna JC and Carrera MV. Down-regulation of acyl-CoA oxidase gene expression and increased NF-kappaB activity in etomoxir-induced cardiac hypertrophy. J Lipid Res 2003; 44: 388-398.

[14] Hu J, Wang H, Li X, Liu Y, Mi Y, Kong H, Xi D, Yan W, Luo X, Ning Q and Wang X. Fibrinogen-like protein 2 aggravates nonalcoholic steatohepatitis via interaction with TLR4, eliciting inflammation in macrophages and inducing hepatic lipid metabolism disorder. Theranostics 2020; 10: 9702-9720.

[15] Han H, Guo Y, Li X, Shi D, Xue T, Wang L, Li Y and Zheng M. Plant sterol ester of α-linolenic acid attenuates nonalcoholic fatty liver disease by rescuing the adaption to endoplasmic reticulum stress and enhancing mitochondrial biogenesis. Oxid Med Cell Longev 2019; 2019: 8294141.

[16] O'Connor RS, Guo L, Ghassemi S, Snyder NW, Worth AJ, Weng L, Kam Y, Philipson B, Trefely S, Nunez-Cruz S, Blair IA, June CH and Milone MC. The CPT1a inhibitor, etomoxir induces severe oxidative stress at commonly used concentrations. Sci Rep 2018; 8: 6289.

[17] Kalucka J, Bierhansl L, Conchinha NV, Missiaen R, Elia I, Brüning U, Scheinok S, Treps L, Cantelmo AR, Dubois C, de Zeeuw P, Goveia J, Zecchin A, Taverna F, Morales-Rodriguez F, Brajic A, Conradi LC, Schoors S, Harjes U, Vriens K, Pilz GA, Chen R, Cubbon R, Thienpont B, Cruys B, Wong BW, Ghesquière B, Dewerchin M, De Bock K, Sagaert X, Jessberger S, Jones EAV, Gallez B, Lambrechts D, Mazzone M, Eelen G, Li X, Fendt SM and Carmeliet P. Quiescent endothelial cells upregulate fatty acid β-oxidation for vasculoprotection via redox homeostasis. Cell Metab 2018; 28: 881-894, e13.

[18] Chen N, Mu L, Yang Z, Du C, Wu M, Song S, Yuan C and Shi Y. Carbohydrate response element-binding protein regulates lipid metabolism via mTOR complex1 in diabetic nephropathy. J Cell Physciol 2021; 236: 625-640.

[19] Portilla D. Role of fatty acid beta-oxidation and calcium-independent phospholipase A2 in ischemic acute renal failure. Curr Opin Nephrol Hypertens 1999; 8: 473-477.

[20] Zager RA, Johnson AC and Hanson SY. Renal tubular triglyercide accumulation following endotoxic, toxic, and ischemic injury. Kidney Int 2005; 67: 111-121.

[21] Lan R, Geng H, Singha PK, Saikumar P, Bottinger EP, Weinberg JM and Venkatachalam MA. Mitochondrial pathology and glycolytic shift during proximal tubule atrophy after ischemic AKI. J Am Soc Nephrol 2016; 27: 3356-3367.

[22] Druilhet RE, Overturf ML and Kirkendall WM. Cortical and medullary lipids of normal and nephrosclerotic human kidney. Int J Biochem 1978; 9: 729-734.

[23] Rouser G, Simon G and Kritchevsky G. Species variations in phospholipid class distribution of organs. I. Kidney, liver and spleen. Lipids 1969; 4: 599-606.

[24] Simon N and Hertig A. Alteration of fatty acid oxidation in tubular epithelial cells: from acute kidney injury to renal fibrogenesis. Front Med (Lausanne) 2015; 2: 52.

[25] Lynch MR, Tran MT and Parikh SM. PGC1α in the kidney. Am J Physiol Renal Physiol 2018; 314: F1-F8.

[26] Lee G, Uddin MJ, Kim Y, Ko M, Yu I and Ha H. PGC-1α, a potential therapeutic target against kidney aging. Aging Cell 2019; 18: e12994.

[27] Portilla D, Dai G, McClure T, Bates L, Kurten R, Megyesi J, Price P and Li S. Alterations of PPARalpha and its coactivator PGC-1 in cisplatin-induced acute renal failure. Kidney Int 2002; 62: 1208-1218.

[28] Tran M, Tam D, Bardia A, Bhasin M, Rowe GC, Kher A, Zsengeller ZK, Akhavan-Sharif MR, Khankin EV, Saintgeniez M, David S, Burstein D, Karumanchi SA, Stillman IE, Arany Z and Parikh SM. PGC-1α promotes recovery after acute kidney injury during systemic inflammation in mice. J Clin Invest 2011; 121: 4003-4014.

[29] Lempiäinen J, Finckenberg P, Mervaala EE, Sankari S, Levijoki J and Mervaala EM. Caloric restriction ameliorates kidney ischaemia/reperfusion injury through PGC-1α-eNOS pathway and enhanced autophagy. Acta Physiol (Oxf) 2013; 208: 410-421.

[30] Zhang LN, Zhou HY, Fu YY, Li YY, Wu F, Gu M, Wu LY, Xia CM, Dong TC, Li JY, Shen JK and Li J. Novel small-molecule PGC-1α transcriptional regulator with beneficial effects on diabetic db/db mice. Diabetes 2013; 62: 1297-1307.

[31] Xu Y, Kabba JA, Ruan W, Wang Y, Zhao S, Song X, Zhang L, Li J and Pang T. The PGC-1α activator ZLN005 ameliorates ischemia-induced neuronal injury in vitro and in vivo. Cell Mol Neurobiol 2018; 38: 929-939.

[32] Fu ZJ, Wang ZY, Xu L, Chen XH, Li XX, Liao WT, Ma HK, Jiang MD, Xu TT, Xu J, Shen Y, Song B, Gao PJ, Han WQ and Zhang W. HIF-1α-BNIP3-mediated mitophagy in tubular cells protects against renal ischemia/reperfusion injury. Redox Biol 2020; 36: 101671.

[33] Wen D, Zou YF, Gao YH, Zhao Q, Xie YY, Shen PY, Xu YW, Xu J, Chen YX, Feng XB, Shi H and Zhang W. Inhibitor of DNA binding 1 is induced during kidney ischemia-reperfusion and is critical for the induction of hypoxia-inducible factor-1α. Biomed Res Int 2016; 2016: 4634386.

[34] Ou MX, Song YX, Li SJ, Liu GY, Jia JY, Zhang MQ, Zhang HC and Yu C. LC-MS/MS method for serum creatinine: comparison with enzymatic method and Jaffe method. PLoS One 2015; 10: e0133912.

[35] Zhang D, Liu Y, Wei Q, Huo Y, Liu K, Liu F and Dong Z. Tubular p53 regulates multiple genes to mediate AKI. J Am Soc Nephrol 2014; 25: 2278-2289.

[36] Nakamura MT, Yudell BE and Loor JJ. Regulation of energy metabolism by long-chain fatty acids. Prog Lipid Res 2014; 53: 124-144.

[37] Hernández-Gea V, Ghiassi-Nejad Z, Rozenfeld R, Gordon R, Fiel MI, Yue Z, Czaja MJ and Friedman SL. Autophagy releases lipid that promotes fibrogenesis by activated hepatic stellate cells in mice and in human tissues. Gastroenterology 2012; 142: 938-946.

[38] Raud B, Roy DG, Divakaruni AS, Tarasenko TN, Franke R, Ma EH, Samborska B, Hsieh WY, Wong AH, Stüve P, Arnold-Schrauf C, Guderian M, Lochner M, Rampertaap S, Romito K, Monsale J, Brönstrup M, Bensinger SJ, Murphy AN, McGuire PJ, Jones RG, Sparwasser T and Berod L. Etomoxir actions on regulatory and memory T cells are independent of Cpt1a-mediated fatty acid oxidation. Cell Metab 2018; 28: 504-515, e7.

[39] Kang HM, Ahn SH, Choi P, Ko YA, Han SH, Chinga F, Park AS, Tao J, Sharma K, Pullman J, Bottinger EP, Goldberg IJ and Susztak K. Defective fatty acid oxidation in renal tubular epithelial cells has a key role in kidney fibrosis development. Nat Med 2015; 21: 37-46.

[40] Czabotar PE, Lessene G, Strasser A and Adams JM. Control of apoptosis by the BCL-2 protein family: implications for physiology and therapy. Nat Rev Mol Cell Biol 2014; 15: 49-63.

[41] Kaufmann T, Schinzel A and Borner C. Bcl-w(edding) with mitochondria. Trends Cell Biol 2004; 14: 8-12.

[42] Weinberg JM. The cell biology of ischemic renal injury. Kidney Int 1991; 39: 476-500.

[43] Wei Q, Xiao X, Fogle P and Dong Z. Changes in metabolic profiles during acute kidney injury and recovery following ischemia/reperfusion. PLoS One 2014; 9: e106647.

[44] Idrovo JP, Yang WL, Nicastro J, Coppa GF and Wang P. Stimulation of carnitine palmitoyltransferase 1 improves renal function and at-

tenuates tissue damage after ischemia/reperfusion. J Surg Res 2012; 177: 157-164.
[45] Kadlec AO, Chabowski DS, Ait-Aissa K, Hockenberry JC, Otterson MF, Durand MJ, Freed JK, Beyer AM and Gutterman DD. PGC-1α (peroxisome proliferator-activated receptor γ coactivator 1-α) overexpression in coronary artery disease recruits NO and hydrogen peroxide during flow-mediated dilation and protects against increased intraluminal pressure. Hypertension 2017; 70: 166-173.
[46] Zhang T and Liu CF. Overexpression of peroxisome proliferator-activated receptor γ coactivator 1-α protects cardiomyocytes from lipopolysaccharide-induced mitochondrial damage and apoptosis. Inflammation 2020; 43: 1806-1820.
[47] Li W, Li X, Wang B, Chen Y, Xiao A, Zeng D, Ou D, Yan S, Li W and Zheng Q. ZLN005 protects cardiomyocytes against high glucose-induced cytotoxicity by promoting SIRT1 expression and autophagy. Exp Cell Res 2016; 345: 25-36.
[48] Li M and Li CM. Sirt3 modulates fatty acid oxidation and attenuates cisplatin-induced AKI in mice. J Cell Mol Med 2020; 24: 5109-5121.
[49] Lesnefsky EJ, Chen Q, Tandler B and Hoppel CL. Mitochondrial dysfunction and myocardial ischemia-reperfusion: implications for novel therapies. Annu Rev Pharmacol Toxicol 2017; 57: 535-565.
[50] Oh CJ, Ha CM, Choi YK, Park S, Choe MS, Jeoung NH, Huh YH, Kim HJ, Kweon HS, Lee JM, Lee SJ, Jeon JH, Harris RA, Park KG and Lee IK. Pyruvate dehydrogenase kinase 4 deficiency attenuates cisplatin-induced acute kidney injury. Kidney Int 2017; 91: 880-895.
[51] Wu H, Liu B, Chen Z, Li G and Zhang Z. MSC-induced lncRNA HCP5 drove fatty acid oxidation through miR-3619-5p/AMPK/PGC1α/CEBPB axis to promote stemness and chemoresistance of gastric cancer. Cell Death Dis 2020; 11: 233.
[52] Du Q, Tan Z, Shi F, Tang M, Xie L, Zhao L and Li Y. PGC1α/CEBPB/CPT1A axis promotes radiation resistance of nasopharyngeal carcinoma through activating fatty acid oxidation. Cancer Sci 2019; 110: 2050-2062.
[53] Han J and Kaufman RJ. The role of ER stress in lipid metabolism and lipotoxicity. J Lipid Res 2016; 57: 1329-1338.
[54] Xu J and Taubert S. Beyond proteostasis: lipid metabolism as a new player in ER homeostasis. Metabolities 2021; 11: 52.